



Effect of Dam Emplacement and Water Level Changes on Sublacustrine Geomorphology and Recent Sedimentation in Jackson Lake, Grand Teton National Park (Wyoming, United States)

Michael M. McGlue*, John R. Dilworth, Hillary L. Johnson, Samuel J. Whitehead, J. Ryan Thigpen, Kevin M. Yeager, Edward W. Woolery, Summer J. Brown, Sarah E. Johnson, Cooper S. Cearley, Gillian M. Clark, T. Spencer Dixon, Ryan C. Goldsby, Autumn L. Helfrich, Bailee N. Hodelka, Edward L. Lo, Leandro Domingos-Luz, Nicholas E. Powell, Giliane G. Rasbold and William R. Swanger

Department of Earth and Environmental Sciences, University of Kentucky, Lexington, KY, United States

OPEN ACCESS

Edited by:

Rachel Brackenridge,
University of Aberdeen,
United Kingdom

Reviewed by:

Michael Hofmann,
University of Montana, United States
Sabrina Brown,
Defiance College, United States

*Correspondence:

Michael M. McGlue
michael.mcglue@uky.edu

Received: 17 July 2022

Accepted: 03 January 2023

Published: 17 January 2023

Citation:

McGlue MM, Dilworth JR, Johnson HL, Whitehead SJ, Thigpen JR, Yeager KM, Woolery EW, Brown SJ, Johnson SE, Cearley CS, Clark GM, Dixon TS, Goldsby RC, Helfrich AL, Hodelka BN, Lo EL, Domingos-Luz L, Powell NE, Rasbold GG and Swanger WR (2023) Effect of Dam Emplacement and Water Level Changes on Sublacustrine Geomorphology and Recent Sedimentation in Jackson Lake, Grand Teton National Park (Wyoming, United States). *Earth Sci. Syst. Soc.* 3:10066. doi: 10.3389/esss.2023.10066

Dam installation on a deep hydrologically open lake provides the experimental framework necessary to study the influence of outlet engineering and changing base levels on limnogeological processes. Here, high-resolution seismic reflection profiles, sediment cores, and historical water level elevation datasets were employed to assess the recent depositional history of Jackson Lake, a dammed glacial lake located adjacent to the Teton fault in western Wyoming (USA). Prograding clinofolds imaged in the shallow stratigraphy indicate a recent lake-wide episode of delta abandonment. Submerged ~11–12 m below the lake surface, these Gilbert-type paleo-deltas represent extensive submerged coarse-grained deposits along the axial and lateral margins of Jackson Lake that resulted from shoreline transgression following dam construction in the early 20th century. Other paleo-lake margin environments, including delta plain, shoreline, and glacial (drumlins, moraines) landforms were likewise inundated following dam installation, and now form prominent features on the lake floor. In deepwater, a detailed chronology was established using ¹³⁷Cs, ²¹⁰Pb, and reservoir-corrected ¹⁴C for a sediment core that spans ~1654–2019 Common Era (CE). Dam emplacement (1908–1916 CE) correlates with a nearly five-fold acceleration in accumulation rates and a depositional shift towards carbonaceous sediments. Interbedded organic-rich black diatomaceous oozes and tan silts track changes in reservoir water level elevation, which oscillated in response to regional climate and downstream water needs between 1908 and 2019 CE. Chemostratigraphic patterns of carbon, phosphorus, and sulfur are consistent with a change in nutrient status and productivity, controlled initially by transgression-driven flooding of supralittoral soils and vegetation, and subsequently with water level changes. A thin gravity flow deposit punctuates the deepwater strata and provides a benchmark for turbidite

characterization driven by hydroclimate change. Because the Teton fault is a major seismic hazard, end-member characterization of turbidites is a critical first step for accurate discrimination of mass transport deposits controlled by earthquakes in more ancient Jackson Lake strata. Results from this study illustrate the influence of dam installation on sublacustrine geomorphology and sedimentation, which has implications for lake management and ecosystem services. Further, this study demonstrates that Jackson Lake contains an expanded, untapped sedimentary archive recording environmental changes in the American West.

Keywords: climate change, dam, lake sediment, limnogeology, reservoir, seismic reflection, sedimentary geochemistry, Snake River

INTRODUCTION

Dams are an important component of the global infrastructure used to modify watersheds to control flooding, regulate sediment budgets, store water for irrigation, or generate hydropower (e.g., Graf, 1999). Dam construction can alter: 1) downstream discharge and river channel habit, 2) the composition and texture of fluvial, lacustrine, deltaic, and estuarine sediments, 3) nutrient fluxes and biogeochemical cycling, and 4) population dynamics of flora and fauna by constricting habitats and migration pathways (e.g., Snyder et al., 2004; Cintra-Buenrostro et al., 2005; Persico and Meyer, 2013; Sawakuchi et al., 2015; Maavara et al., 2020). Thus, modification of inland waters by dams is a profound mechanism of aquatic ecosystem engineering and a hallmark of the Anthropocene (Ligon et al., 1995; Poff et al., 2007; Merritts et al., 2011). Dams may also pose hazards in seismically active areas where earthquakes could result in failure or tsunamis (Chopra, 1968; Kremer et al., 2012). Nevertheless, dams are an integral aspect of water management around the world, and have a particularly long and well-scrutinized history in the western USA. In Wyoming (USA), Jackson Lake Dam was the first major structure built by the Minidoka Project to improve irrigation in the upper Snake River Valley (**Figure 1**) (Stene, 1997). Freshwater from the Snake River was key for sustaining the burgeoning agricultural economies of several states in the headwaters of the Columbia River in the late 19th and early 20th centuries. An initial dam was built over the lake's natural outlet in 1908, and a series of modifications designed to improve structural fidelity were finalized by 1916. Dam completion resulted in a ~12 m transgression of Jackson Lake, and the reservoir stores ~847,000 acre-ft of freshwater with a full pool elevation of 6,769 ft. (2,063 m.) above mean sea level (amsl; Stene, 1997). Today, the reservoir sustains crops and pasturelands valued at > \$500M/yr, and is a recreational centerpiece for Grand Teton National Park.

Reservoirs act as sinks on the landscape, and as such they are valuable archives of catchment and atmospheric particulates when undisturbed by sediment management practices such as dredging or onshore erosion controls (Shotbolt et al., 2005). From a stratigraphic perspective, dam installation at Jackson Lake provides a chronological

datum for examining the tempo and mode of changes to an overfilled lacustrine basin (*sensu* Carroll and Bohacs, 1999) due to oscillations in base level. Resolving the influences of water level changes on Jackson Lake is crucial not only for a thorough understanding of the depositional system, but also for gaining insight on how ecosystem services from the lake respond to environmental changes (e.g., Xu et al., 2017). Monitoring by the U.S. Bureau of Reclamation since dam installation affords access to a water level elevation dataset extending to the present day (**Figure 2A**). In addition, early geodetic maps of western Wyoming provide a snapshot of Jackson Lake's length:width, island distribution, outlet configuration, and proximity to adjacent Teton range topography prior to its conversion into a reservoir (**Figure 2B**). These boundary conditions and data motivate our study, which seeks to use Jackson Lake as a natural laboratory to assess limnogeological processes associated with dam installation. Here, high-resolution historical records of water level, paired with Compressed High Intensity Radar Pulse (CHIRP) seismic reflection profiles and well-dated sediment cores, allow a precise examination of how environmental changes of the last several centuries influenced Jackson Lake. Importantly, the seismic hazard in this region is considered high, in part because no earthquakes have been recorded along the active Teton fault in the recent past (<5 Kyr; Larsen et al., 2019; DuRoss et al., 2021). Therefore, calibration of the sedimentary history of Jackson Lake may also provide the opportunity to resolve fault slip deficits, as the Holocene and Pleistocene strata may preserve a much more sensitive record of paleo-earthquake activity (e.g., Strasser et al., 2013; Moernaut et al., 2017; Larsen et al., 2019).

STUDY SITE

Jackson Lake is the largest (~100 km²) of several glacial lakes situated adjacent to the high-relief, seismically active Teton normal fault, a Miocene-aged structure that evolved with Basin and Range extension and Yellowstone hotspot activity (Brown et al., 2017; Thigpen et al., 2021) (**Figures 2C, D**). The Snake River flows into northern Jackson Lake and smaller underfit drainages enter along the basin's western transverse margin

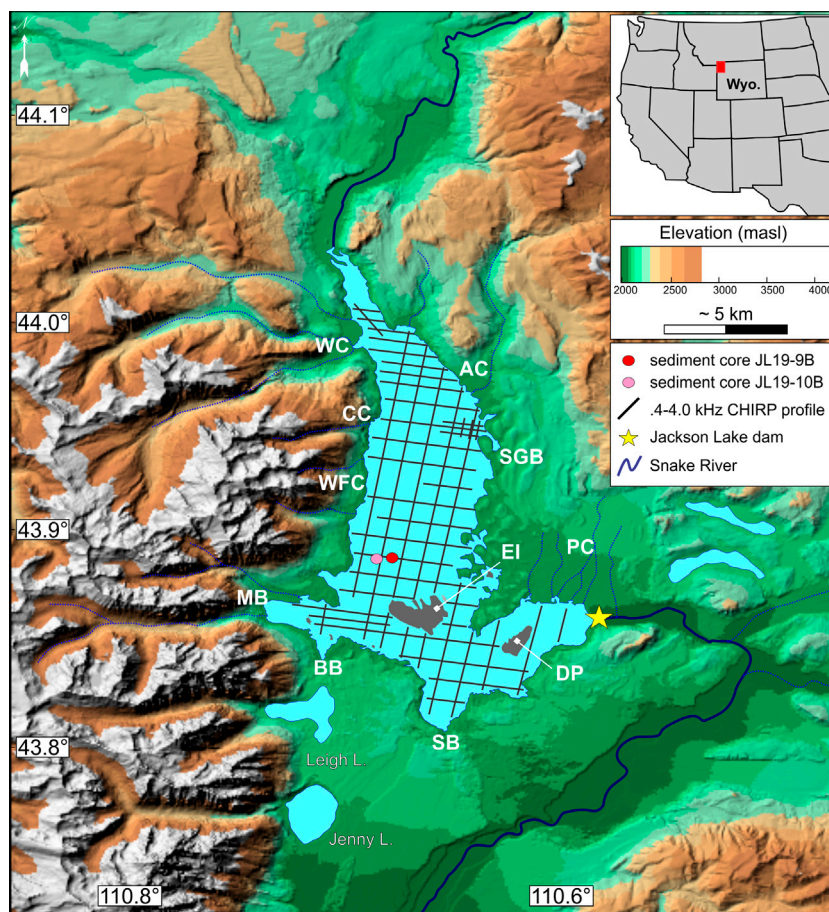


FIGURE 1 | Digital elevation map of the study area. Jackson Lake (blue) sits adjacent to high topography formed by the Teton fault. The Snake River enters Jackson Lake from the north, and exits on the southeast margin via the Jackson Lake dam (marked by a yellow star). Note spatial coverage of seismic reflection profiles and sediment cores used in this study. WC, Webb Canyon. CC, Colter Canyon. WFC, Waterfalls Canyon. MB, Moran Bay. BB, Bearpaw Bay. SB, Spaulding Bay. DP, Donoho Point. EI, Elk Island. PC, Pilgrim/Second Creek. SGB, Sargents Bay. AC, Arizona Creek.

(Figure 1). Although large rivers entering the lake on its eastern margin are absent, the overall hydrological configuration of Jackson Lake shares similarities to many exorheic rift lakes (Gawthorpe and Leeder, 2000). Today, the Snake River flows out through a concrete spillway on Jackson Lake Dam, located at the southeastern margin of Jackson Lake (Figure 1). Climate of the region falls in the Dsc Köppen class (dry-summer subarctic) and is characterized by cold wet winters and dry summers, though intense rains may occur in the summer months as storm fronts interact with the alpine topography. Little published limnological information exists for the lake, apart from some limited physical and chemical data. Nutrient and productivity measurements detailed in Kilham et al. (1996) suggest that Jackson Lake is mesotrophic, an inference confirmed by diatom assemblages detailed in a companion paper (Dilworth et al., submitted).

The Jackson Lake watershed is dominated by metasedimentary and volcanoclastic rocks that make up the Teton Range, Absaroka Mountains, and Yellowstone Plateau (Love et al., 1978; Christiansen, 2001). Most geological

descriptions of Jackson Lake focus on its development due to southerly flow of glacial ice from the Yellowstone Plateau in the Pleistocene (Licciardi and Pierce, 2018 and references therein). Far less is known about the limnogeology of the extant basin and the effects of dam construction on the aquatic ecosystem, though several studies have examined downstream changes in the Snake River owing to outlet engineering (Marston et al., 2005; Nelson et al., 2013). Early Jackson Lake sediment core studies yielded insights on the diatom flora, as well as estimates of offshore sedimentation rates based on magnetic properties (Shuey et al., 1977; Kilham et al., 1996). Archeological surveys, conducted when water levels were much reduced in the 1980s, identified hearths and potsherds that confirmed occupation of paleo-beaches by indigenous people in the Holocene (Connor, 1998). Prior geophysical surveys produced several vintages of low-resolution subsurface images that suggested the presence of ancient shorelines or fault geometries, but issues associated with image quality or navigation prevented complete characterization of the basin fill, thus most of the

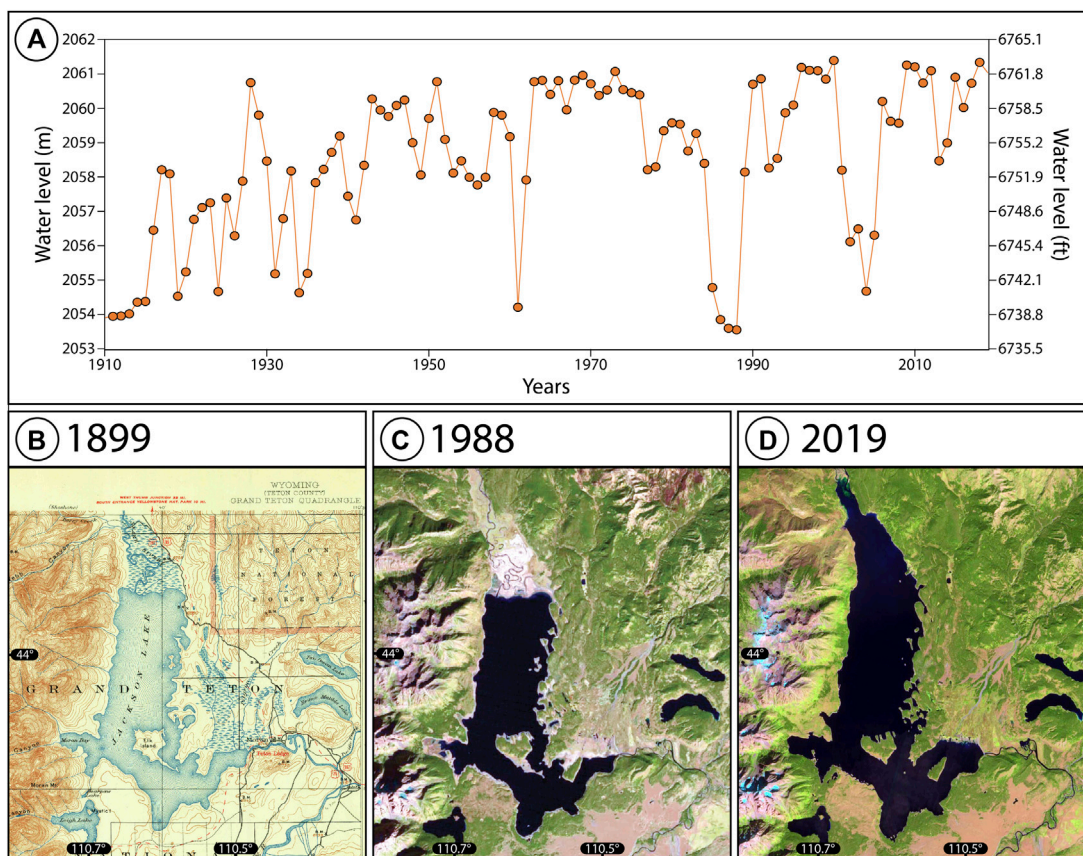


FIGURE 2 | (A) Mean annual water level elevation for Jackson Lake, 1910–2019 Common Era. Data are publicly available from the US Bureau of Reclamation HYDROMET network (<https://www.usbr.gov/pn/hydromet/arcread.html>). Note significant variability (up to ~10 m) in reservoir level associated with drought and/or dam repair during the period of record. **(B)** Historical geodetic map of Jackson Lake (U.S. Geological Survey, 1899) showing lake morphology and the extent of the Snake River delta prior to dam installation. **(C, D)** Landsat imagery of the study site in 1988 and 1999, illustrating contrasting water levels and lake morphology at lowstand versus highstand. The extent and position of the Snake River delta is strongly influenced by the presence of the dam and changes in water level elevation.

lake's subsurface remains unexplored (Pierce and Colman, 1986; Smith et al., 1993).

METHODS AND MATERIALS

Seismic Reflection

A lake-wide (>100 line-km; **Figure 1**) CHIRP sub-bottom profiling survey was completed on Jackson Lake in 2018 CE using an Edgetech 3200 XS acquisition system paired with a SB-0512i towfish operating at a frequency of 0.4–4.0 kHz (**Table 1**). Seismic signals were analyzed using HYPACK Sub-Bottom and Seisware software. Data quality ranged from good to excellent, yielding seismic signals with ~12 cm vertical resolution assuming the $\frac{1}{4}$ wavelength rule (e.g., Sheriff, 1977). The CHIRP data are reported in milliseconds two-way travel time (ms TWTT) and depth conversions utilized a velocity of 1,500 m/s for shallow unconsolidated sediments in hydrostatic equilibrium with the water column (Johnson et al., 2022). The focus of the CHIRP analysis was sub-lacustrine geomorphology and contemporary sedimentary

TABLE 1 | CHIRP seismic acquisition and processing parameters.

| | |
|---------------------|---|
| Acquisition system | Edgetech 3200-XS |
| Source and receiver | Edgetech SB-512i |
| Source depth | 0.5 m |
| Power | 2000 W |
| Frequency | 0.4–4.0 kHz |
| Pulse length | 5 ms |
| Sampling rate | 40 kHz |
| Navigation | Globalsat BU-353S4 USB GPS |
| Processing | Notch filter, time varying gain, top mute |

processes. A bathymetric map was produced by tracing the water-sediment interface across the basin, and generating an interpolated grid and contour set within Seisware. Acoustic basement was defined as the level below which the stratigraphy could not be resolved by the CHIRP system. All mapping honored the location of major faults, which were interpreted on the basis of offset reflections on the acoustic basement horizon. The total thickness of seismically resolvable strata was determined by creating an isopach

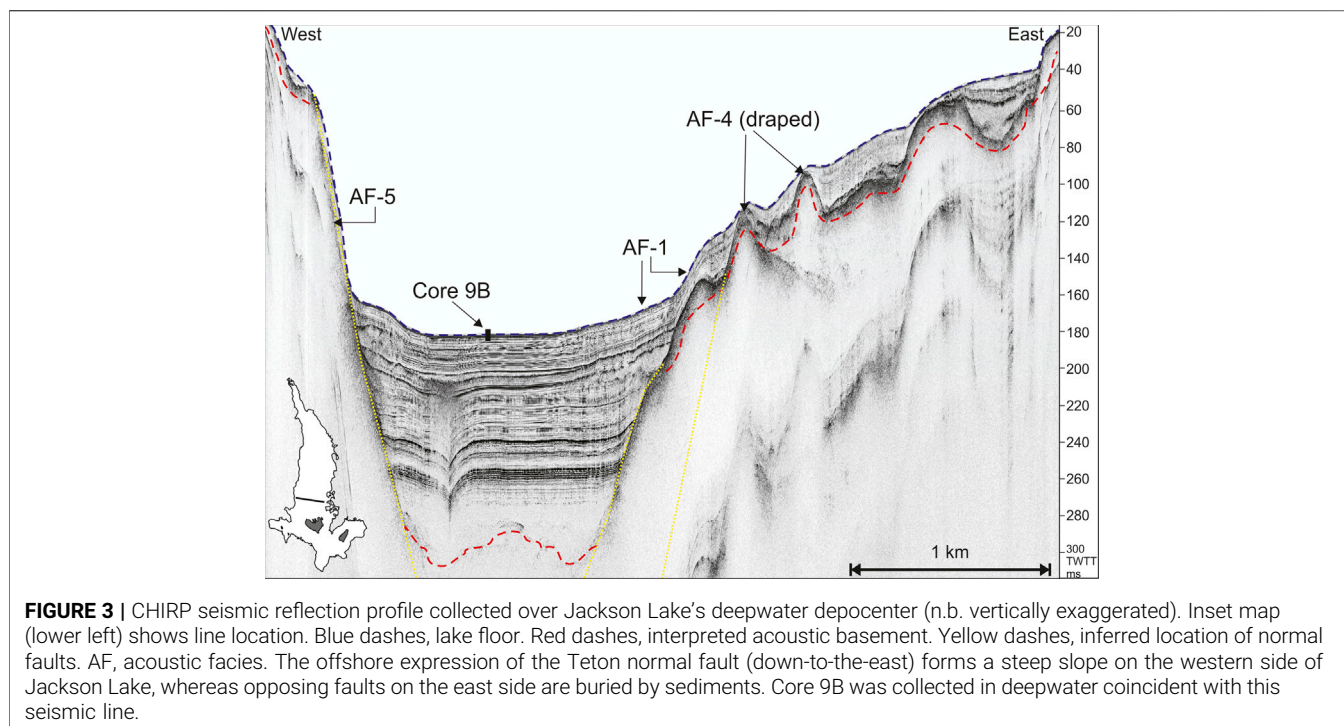


FIGURE 3 | CHIRP seismic reflection profile collected over Jackson Lake's deepwater depocenter (n.b. vertically exaggerated). Inset map (lower left) shows line location. Blue dashes, lake floor. Red dashes, interpreted acoustic basement. Yellow dashes, inferred location of normal faults. AF, acoustic facies. The offshore expression of the Teton normal fault (down-to-the-east) forms a steep slope on the western side of Jackson Lake, whereas opposing faults on the east side are buried by sediments. Core 9B was collected in deepwater coincident with this seismic line.

map in Seisware, utilizing the acoustic basement and lake floor horizons. Lake floor acoustic facies within a ~ 10 ms TWTT window around the water bottom return were also mapped to identify features indicative of recent lake level change (e.g., Scholz et al., 1990).

Core Facies

Two short (<60 cm) sediment cores were collected by hand from Jackson Lake using an UWITECTM gravity corer in 2019 CE (Figure 1). The coring locations were informed by analysis of seismic reflection profiles, which showed undisturbed lake floor deposits above a deepwater depocenter (Figure 3). These cores are archived under the names GTGC-JL19-9B-1G-1-A and GTGC-JL19-10B-1G-1-A, respectively. GTGC-JL19-9B-1G-1-A (core 9B) was collected at $\sim 43.889^\circ\text{N}$ latitude, 110.699°W longitude, whereas GTGC-JL19-10B-1G-1-A (core 10B) was collected at $\sim 43.889^\circ\text{N}$ latitude, 110.695°W longitude. The sediment-water interface was retrieved intact for both cores. Cores were stabilized in the field using floral foam, sealed, and shipped to the U.S. Continental Scientific Drilling Facility (CSD) for processing. At the CSD, the cores were split, imaged, and scanned for physical properties on GEOTEK multi-sensor and XYZ magnetic susceptibility loggers; we focused on magnetic susceptibility (MS) and the gamma-ray attenuation porosity estimator (GRAPE) in this study. MS and GRAPE were measured at 0.5-cm increments downcore. Core sediments were described using standard techniques, including microscopic analysis of smear slides and screen-washed residues (Schnurrenberger et al., 2003).

Core Chronology

The upper ~ 30 cm of both cores were sub-sampled at 1-cm intervals to establish recent chronology using the short-lived radionuclides ^{137}Cs (half-life = 30 yr.) and ^{210}Pb (half-life = 22.3 yr.) (e.g., Yeager et al., 2004). Gamma spectrometry was used to measure ^{137}Cs activity with Canberra High Purity Germanium well detectors and DSA-1000 multi-channel analyzers at the University of Kentucky. Sediment accumulation rates were calculated using ^{137}Cs by:

$$S = (D_{pk}/t)$$

where S = sediment mass accumulation rate ($\text{g cm}^{-2} \text{yr}^{-1}$), D_{pk} = the mass depth (g cm^{-2}) at which the 1963 peak in ^{137}Cs activity was found, and t = the time (yr.) since 1963 CE, the year that the Partial Nuclear Test Ban Treaty was ratified. Our analysis assumed that the inception of atmospheric fallout was 1952 CE (e.g., Waters et al., 2015).

High-resolution alpha spectrometry was used to determine ^{210}Pb activities via ^{210}Po using model 7200 Canberra integrated alpha spectrometers. Sediment accumulation rates were calculated using excess ^{210}Pb ($^{210}\text{Pb}_{xs}$) and the constant flux-constant sedimentation model of Appleby and Oldfield (1983):

$$[I(z)] = [I(0)]^{(-\alpha t)} \rightarrow \alpha = (\lambda/S)$$

where $[I(z)]$ and $[I(0)] = ^{210}\text{Pb}_{xs}$ at depth z and the sediment-water interface, respectively; S = sediment accumulation rate ($\text{g cm}^{-2} \text{yr}^{-1}$); α = the slope of the best fit line to the semi-log plot of $^{210}\text{Pb}_{xs}$ versus depth, and λ = decay constant ($^{210}\text{Pb} = .031 \text{ yr}^{-1}$).

TABLE 2 | Radiocarbon data for sediment core 9B using acid-insoluble sedimentary organic matter (OM) and a sample of wood.

| Beta ID | Depth (cm) | Material | ¹⁴ C age (yr.) | ¹⁴ C age uncertainty (yr.) | Reservoir corrected ¹⁴ C age (yr.) | δ ¹³ C (‰) | Bacon- derived mean age (cal yr.) | Bacon-derived 2-sigma age (cal yr.) |
|---------|------------|----------|---------------------------|---------------------------------------|---|-----------------------|-----------------------------------|-------------------------------------|
| 566762 | 40 | Wood | 90 | 30 | 90 | -27.0 | 110 | 50–150 |
| 566758 | 40 | OM | 4,310 | 30 | 90 | -26.4 | 110 | 50–150 |
| 566759 | 45 | OM | 4,480 | 30 | 260 | -26.0 | 170 | 90–220 |
| 566760 | 50 | OM | 4,430 | 30 | 210 | -26.0 | 220 | 140–300 |
| 566761 | 55 | OM | 4,680 | 30 | 460 | -25.9 | 280 | 170–360 |

Five samples from the longer of the two cores (core 9B) were radiocarbon (¹⁴C) dated by accelerator mass spectrometry at Beta Analytic Incorporated (Table 2). Four of these samples were fine-grained, organic-rich sediments, and one sample was a charred twig (wood). The wood and one sample of fine-grained sedimentary organic matter (OM) were retrieved from 40 cm down-core; the offset between the ages of these two samples was used to evaluate reservoir effects in Jackson Lake. Bulk sediments were sieved to remove coarse detritus and pretreated with 10% HCl to remove traces of carbonate that could influence the age determinations. The charred twig was pretreated with a sequential acid-base-acid digestion to remove contaminants, and the insoluble material was used in dating. All ¹³⁷Cs, ²¹⁰Pb, and ¹⁴C ages were integrated into a probabilistic age-depth model using Bacon for R (Blaauw and Christen, 2011). The IntCal20 curve (Reimer et al., 2020) was used to convert ¹⁴C years into calibrated years before 1950 CE. The Bacon model parameters included: depth minimum = 0 cm, depth maximum = 57.5 cm, accumulation rate mean 8 yr./cm, section thickness 1.5 cm, and an event bed of instantaneous sedimentation at 13–14 cm. The top of the core was assumed to reflect the year of collection (2019 CE), an inference supported by sedimentation rates established with ¹³⁷Cs and ²¹⁰Pb.

Sediment Geochemistry

Core 9B was sampled every ~.5 cm along its length ($n = 115$), in order to assess the geochemistry of OM accumulating in deepwater sediments. Total organic carbon (TOC) was measured using a LECO SC-144DR carbon determinator at the Kentucky Geological Survey. Samples were decalcified with 10% HCl at room temperature and lyophilized prior to analysis. Three standards (SARM-41, 502-030, 502-630) and replicates of unknowns were measured to assess accuracy and precision, which was better than 1.0%. Total nitrogen (TN) was determined on lyophilized sample splits using a Thermo Finnigan DELTA^{plus} XP elemental analyzer at the University of Kentucky. Sample aliquots for nitrogen analysis were left untreated, to avoid losses of labile organics that can accompany acidification (e.g., Meyers and Ishiwatari, 1993). Precision and accuracy of the TN data, assessed with multiple in-session measurements of a blind standard, was better than .1 wt %. Contributions from inorganic nitrogen were assessed using the cross-plot technique described in Talbot (2002), and a correction factor of .04 wt. % was applied to all values to yield total organic nitrogen (TON). The TOC and TON data were used

to calculate C:N (an indicator of organic matter provenance; Meyers and Ishiwatari, 1993), and values are presented as atomic ratios ([TOC/TON]*1.167).

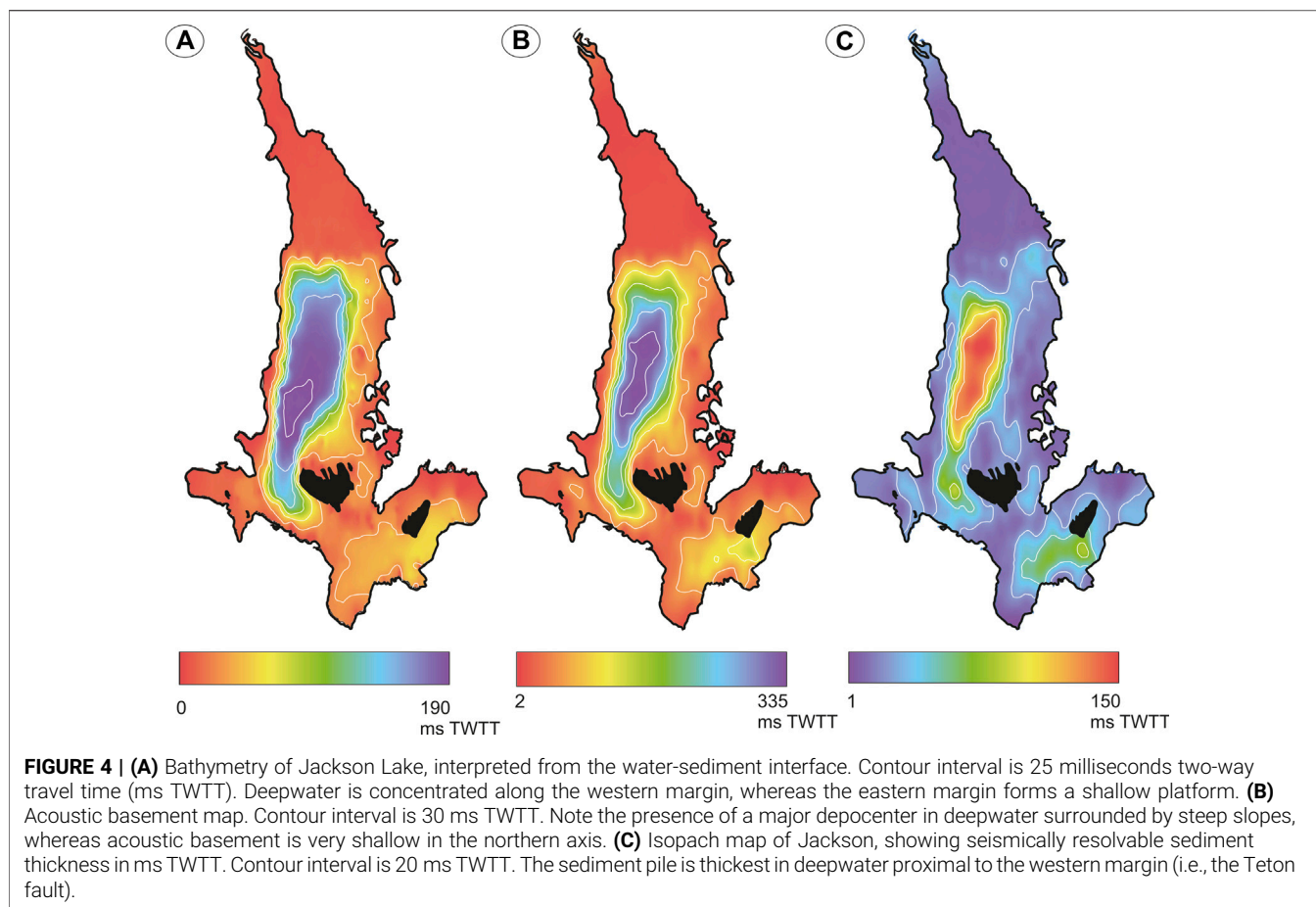
To generate major element chemostratigraphic data, core 9B was scanned along its length (approximately every .5 cm; $n = 111$) using a Cox Analytical Systems ITRAX x-ray fluorescence (XRF) core scanner located at the Large Lakes Observatory, University of Minnesota-Duluth. The scans utilized a Cr source tube run at 30 kV and 55 mA with a 15 s dwell time. All raw data were processed to optimize peak fitting using QSpec 8.6.0 software, and data are presented as counts per second (cps). The elements of interest are associated with detrital minerals, OM, and nutrients (Davies et al., 2015), including: aluminum (Al), silicon (Si), potassium (K), titanium (Ti), phosphorus (P), and sulfur (S). In addition to sediment chemistry, the XRF scanner collected high-resolution x-radiographs, which were employed in the lithostratigraphic analysis to identify variability related to grain density and particle size. All geochemical and physical properties data were analyzed using univariate (wiggle plots) and multivariate (principal components analysis) statistics in the program PAST (Hammer et al., 2001).

RESULTS AND INTERPRETATION

CHIRP Seismic Profiling

Bathymetry and Sediment Distribution Patterns

The bathymetry and acoustic basement maps for Jackson Lake are shown in Figure 4. Jackson Lake is characterized by shallow water depths and gentle lake floor gradients in its northern axis, where the Snake River delta and several smaller lateral drainages (e.g., Moose, Berry, and Arizona Creeks) enter the lake. A south-facing sub-lacustrine slope (~5°) approximately parallel to Colter Canyon marks the transition into a deepwater depocenter, reaching a maximum depth of ~190 ms TWTT (~143 m) during our survey, though this value fluctuates annually due to water level changes. The depocenter is asymmetrical, with some of the deepest areas situated close to the western lake margin (Figure 4A). The asymmetry results from a prominent down-to-the-east normal fault that trends along much of the western flank of the basin, forming a ~12° slope that accumulates minimal sediment (Figure 3). The depocenter is bounded on the eastern side by two down-to-the-west faults that are buried within the sediment pile. These faults create a shallow water platform along the eastern



margin where water depths do not exceed ~ 80 ms TWTT (~ 60 m) (**Figure 4A**). The depocenter tapers to the south, terminating southwest of Elk Island as a furrow with water depths of 130–145 ms TWTT (~ 98 –109 m). In total, the deepwater depocenter is ~ 25 km². Most areas of the lake near the southern shoreline, including Moran Bay, Bearpaw Bay, Spaulding Bay, as well as the Snake River outlet, are low gradient and characterized by relatively shallow water depths (< 80 ms TWTT; < 60 m). The deepest regions near the southern lake shore are found on the east side of Donoho Point (**Figure 4A**).

Acoustic basement contours are arranged very much like isobaths, and together these datasets were used to calculate a CHIRP-resolvable sediment thickness map (**Figures 4B, C**). This isopach reveals two depocenters with relatively thick packages of strata, whereas broad areas characterized by much thinner resolvable strata (< 20 ms TWTT) occur in the northern and southern ends of the lake (**Figure 4C**). Sediment thicknesses reach a maximum of ~ 150 ms TWTT in the deepwater depocenter, just offshore of Waterfalls Canyon; acoustic basement reaches up to ~ 335 ms TWTT in this location (**Figure 4B**). A secondary depocenter is situated along the southeastern lake margin, where the stratal package exceeds ~ 60 ms TWTT. Isopach contours north of the deepwater depocenter reveal an accumulation up to

~ 40 ms TWTT thick south of the Arizona Creek inlet, to the west of Sargents Bay (**Figure 4C**).

Shallow Acoustic Facies

Shallow acoustic facies vary across Jackson Lake (**Table 3**) (**Figure 5**). The deepwater depocenter is dominated by low-moderate amplitude, parallel, continuous reflections (AF-1) that fill accommodation or drape the west-facing normal faults (**Figure 3**). In general, AF-1 reflections do not preferentially thicken towards the west. Tilting of these reflections in the deepwater depocenter, where it occurs, is usually a function of underlying sediment lobes adjacent to faults. Smaller lenses of AF-1 are mappable along the steep slope defining the depocenter's western flank. Subtle changes in gradient along the down-to-the east normal fault control the position of these bi-directionally downlapping lenses of low amplitude, continuous seismic reflectors (**Figure 3**). Given the line spacing of the survey, it remains unclear if these are isolated lenses or a continuous single accumulation. Much of the northern and southern axial margins consist of moderate-high amplitude, parallel, and continuous reflections organized in sheet-like geometries (AF-2). In the northern lake axis, occasional channel incisions and fault offsets are apparent in AF-2, but otherwise these reflections have mostly flat-lying geometries (**Figure 6A**).

TABLE 3 | Shallow acoustic facies characteristics of Jackson Lake.

| Name | External Geometry | Internal acoustic characteristics | Interpretation |
|------|--|---|--|
| AF-1 | Sheet drape, basin fill | Low-moderate amplitude, parallel, continuous | Hemipelagic deposits |
| AF-2 | Tabular, occasional channel cuts and fault offsets | High amplitude, parallel, semi-continuous lake floor return, discontinuous internal reflections | Submerged paleo-floodplain or paleo-lake margin |
| AF-3 | Cliniform | Low-moderate amplitude, sharply oblique to complex sigmoid-oblique, prograding reflections | Paleo-delta deposits |
| AF-4 | Mound | High amplitude, continuous-discontinuous lake floor return, minimal internal reflections | Submerged drumlins or moraines made up of glacial till |
| AF-5 | Slope front | Sharp lake floor return; numerous shallow diffractions | Bedrock fault trace |

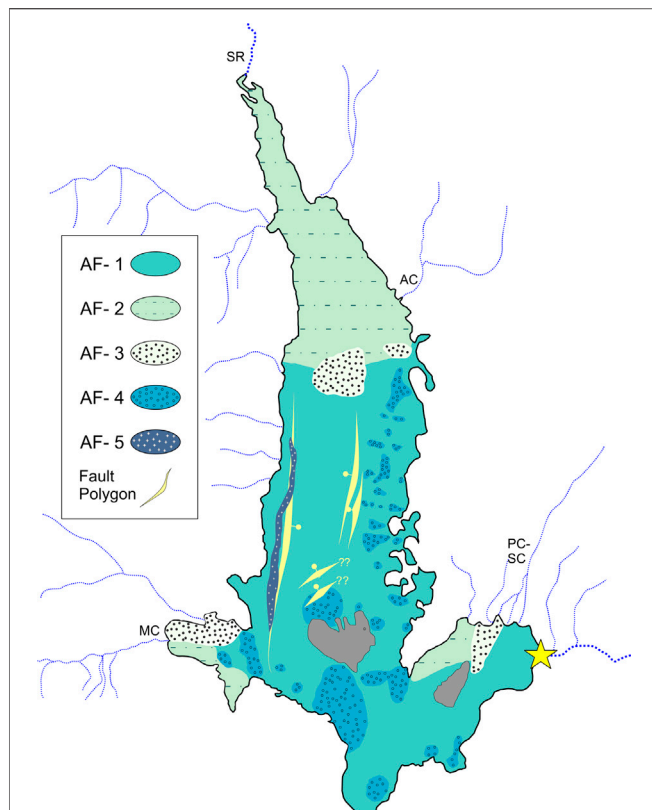


FIGURE 5 | Shallow acoustic facies map for Jackson Lake. AF, acoustic facies. Fault locations (polygons) are marked with cherries on the down-dropped side. Much of the shallow stratigraphy of Jackson Lake consists of low-moderate amplitude, continuous reflections (AF-1), reflecting hemipelagic sedimentation. The lake's northern axis is dominated by AF-2, an acoustic response interpreted to result from flooding of the Snake River delta plain following installation of the dam. Submerged prograding cliniforms (AF-3) are localized in association with the Snake River, as well as Arizona, Moran, and Pilgrim/Second Creeks, and reflect abandoned deltas. Other acoustic facies reflect submerged glacial deposits (drumlins or moraines; AF-4) and the trace of the Teton fault (AF-5). Jackson Lake dam is denoted with a star. SR, Snake River. AC, Arizona Creek. PC, Pilgrim Creek. SC, Second Creek. MC, Moran Creek.

On the southwest side of the basin, submerged cliniforms (AF-3) were found in Moran Bay, <2 km east of the present-day Moran Creek delta (**Figure 7A**). The cliniforms are

oblique, with top-truncated, eastward dipping foreset reflections and a roll-over position at ~15.3 ms TWTT (~11.5 m). The foresets dip at ~6°–7°. These cliniforms are the youngest in a stack that exhibits considerable variability in scale and position (**Figure 7A**). Another stacked set of well-developed oblique to sigmoidal cliniforms is located west of Sargeant's Bay, ~2 km south of the Arizona Creek inlet on the northeast side of the basin (**Figure 7B**). There, top-truncated foreset reflections dip ~3°–5° to the west-southwest, with a roll-over at ~15.2 ms TWTT (~11.4 m). The foreset dips exhibited by the Moran and Arizona Creek cliniforms suggest they are composed of sands that can achieve relatively steep angles of repose (Patruno and Helland-Hansen, 2018). Along the central axis of the basin, a broad sigmoidal-oblique cliniform package with foresets that dip to the south marks the slope break into the deepwater depocenter (**Figure 7C**). Here, the topset-to-foreset roll-over occurs at ~15.2 ms TWTT (~11.4 m). Closer to the dam, a cliniformal package of reflections lies north of Donoho Point, south of the Pilgrim and Second Creek inlets (**Figure 7D**). The internal acoustic stratigraphy of this cliniform was poorly resolved by the CHIRP system, showing only discontinuous high-amplitude reflections. The external form of the package suggests foreset beds dipping approximately to the south, with a roll-over ~14.6 ms TWTT (~11 m). All cliniforms imaged in our CHIRP survey show minimal evidence of sedimentary drape, suggesting these features are geologically young. Grab sampling confirmed that muddy sands dominated at the tops of these features, with gray clayey sands conspicuous on the Snake River cliniform.

The acoustic characteristics of mounds (AF-4) are defined by sharp, high-amplitude returns at the sediment-water interface and minimal internal reflectivity (**Figures 6B, C**). The AF-4 mounds are mainly concentrated along the shallow water eastern platform and are variably draped with sediment or exposed at the lake floor (**Figures 5, 6**). This facies is also found in southern Jackson Lake, and is prominent at the mouth of Moran Bay, forming a ridge between the bay and the deepwater depocenter (Johnson et al., 2022). The characteristics of the slope front facies (AF-5) are defined by a sharp lake floor return directly underlain by numerous shallow diffractions and minimal sub-bottom penetration (**Figure 3**). The AF-5 response is localized along the western lake margin in association with

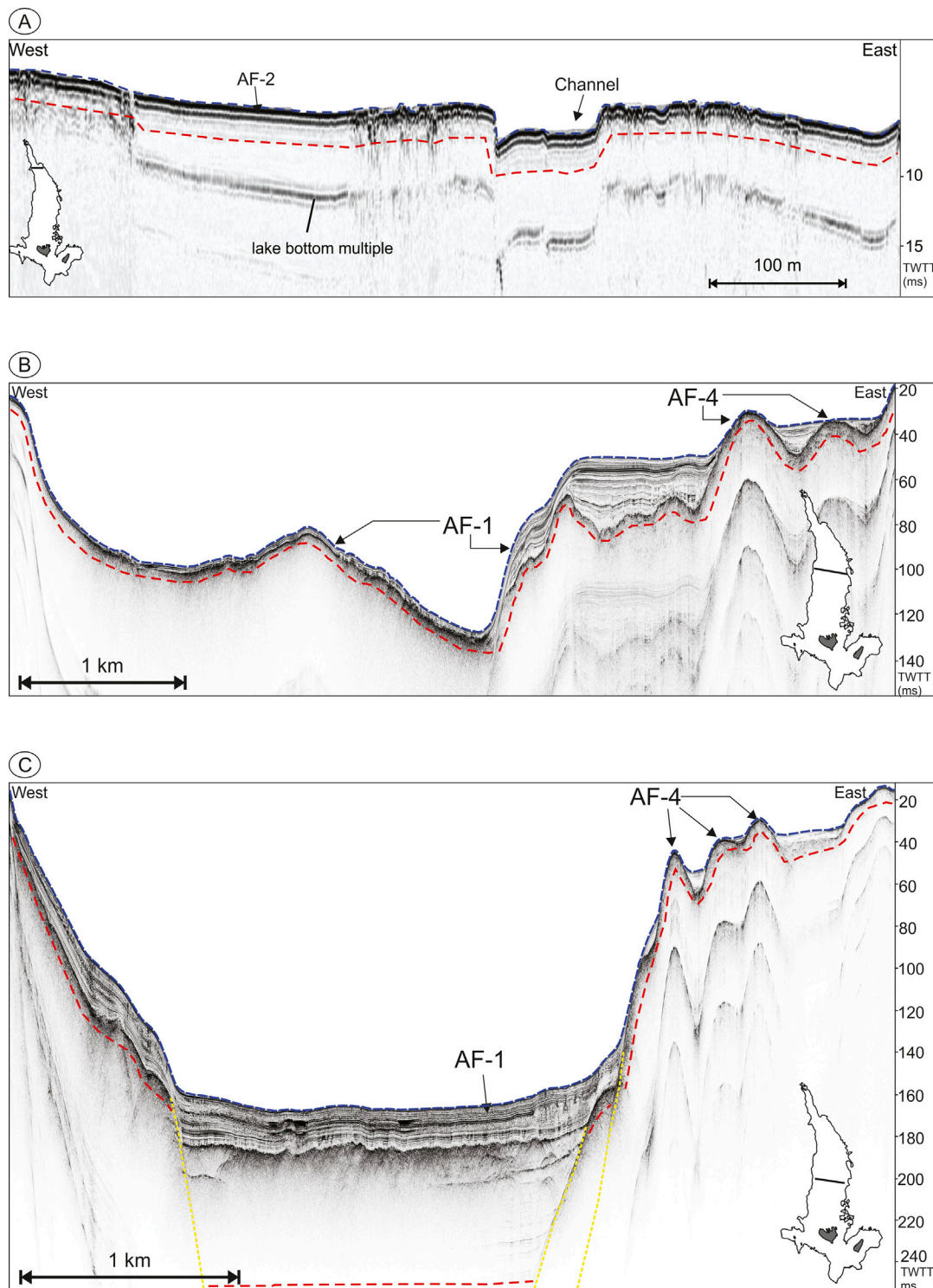
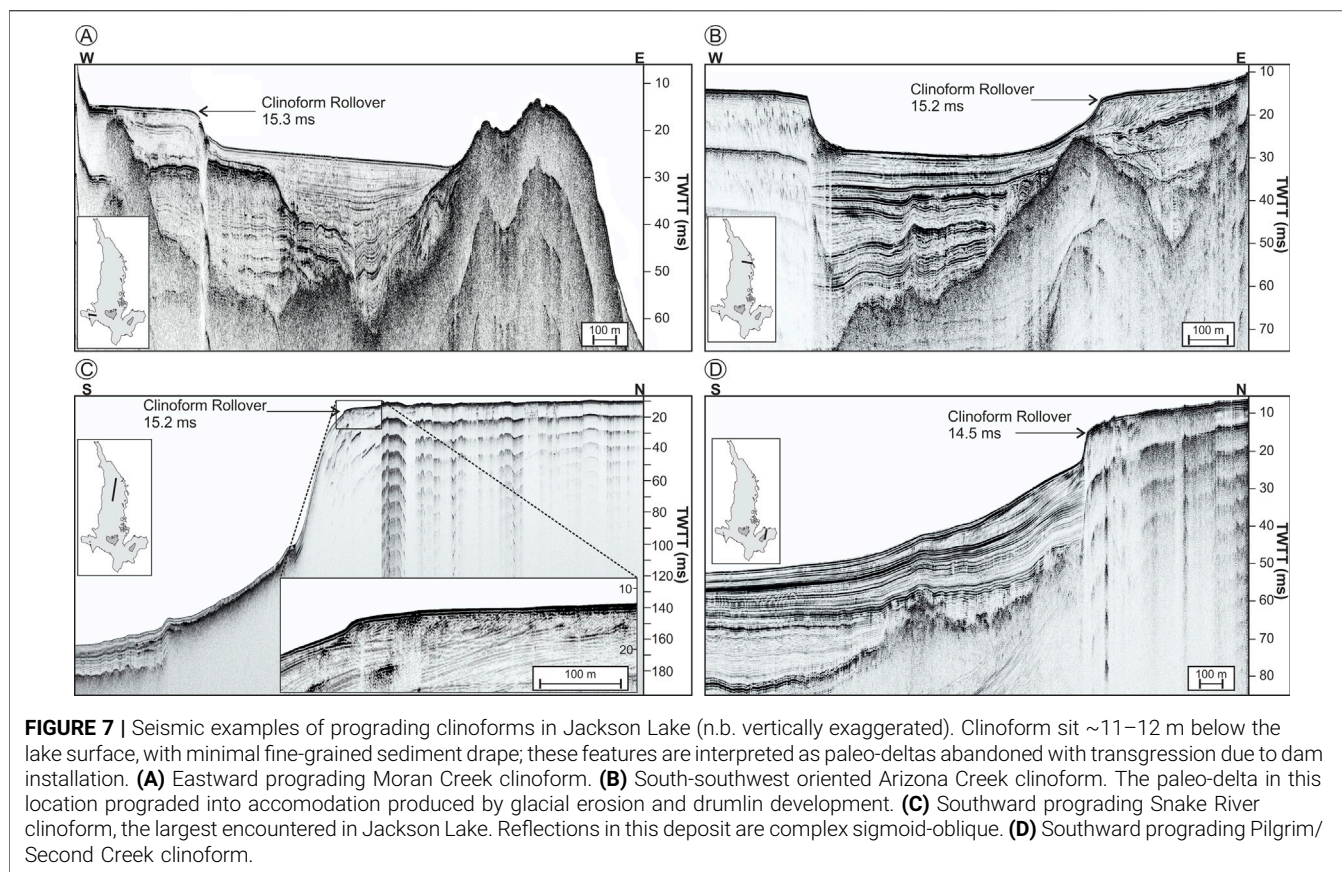


FIGURE 6 | Examples of shallow seismic facies from Jackson Lake. **(A)** CHIRP seismic reflection profile characteristic of northern Jackson Lake, illustrating the AF-2 facies. Signal is limited beneath the high-amplitude water bottom reflection. Note prominent submerged channel cut associated with the Snake River. **(B, C)** West-east oriented seismic profiles from Jackson Lake illustrating AF-1 and AF-4 shallow seismic facies (n.b. vertically exaggerated). Mound-shaped reflections (AF-4) with minimal internal acoustic stratigraphy are concentrated along the shallow eastern platform of Jackson Lake and are interpreted to be of glacial origin. AF-1 is common throughout Jackson Lake; grab sampling and coring confirms the facies to be hemipelagic sediments rich in biogenic silica and detrital silt and clay. Blue dashes, lake floor. Red dashes, interpreted acoustic basement. Yellow dashes, candidate normal fault locations.



the large east-facing normal fault that constrains the deepwater depocenter (**Figures 3, 5**).

Sediment Core Chronology

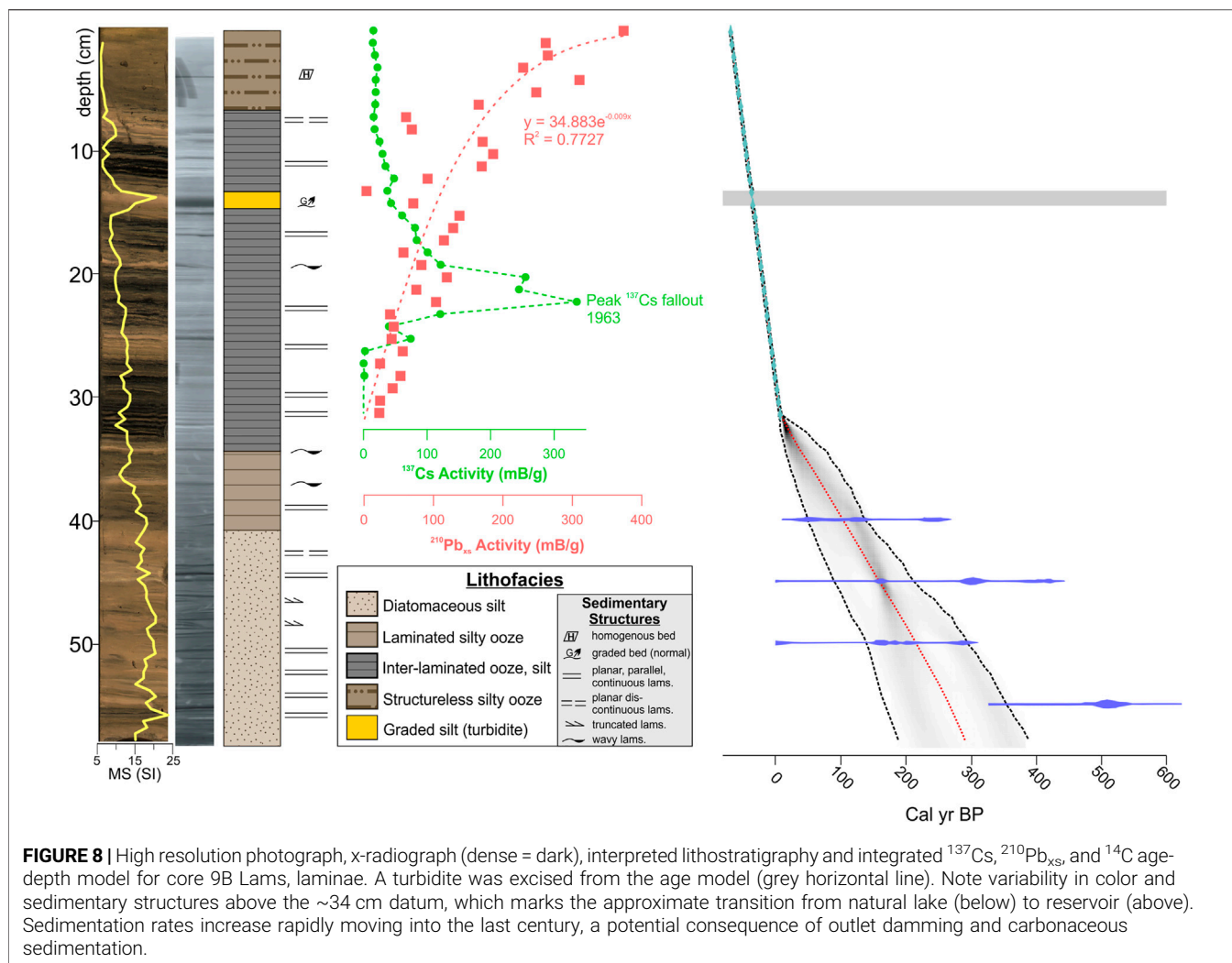
$^{210}\text{Pb}_{\text{xs}}$ activity declines exponentially from the top of core 9B and reaches supported values (<50 mBq/g) at 31 cm (**Figure 9**). $^{210}\text{Pb}_{\text{xs}}$ values yield linear and mass based sediment accumulation rates of $.42 \pm .17$ cm/yr. and $.53 \pm .21$ g cm/yr., respectively. ^{137}Cs activity is first detectable at ~26 cm downcore, and peaks at ~23 cm interpreted to represent the onset of nuclear weapons testing in 1952, and the implementation of the Partial Nuclear Test Ban Treaty on above ground nuclear weapons testing in 1963, respectively. Linear and mass based sediment accumulation rates from ^{137}Cs are $.40 \pm .01$ cm/yr. and $.49 \pm .08$ g cm/yr. Similar ^{210}Pb and ^{137}Cs activities in core 10B suggest reasonably uniform patterns and rates of sedimentation in the deepwater depocenter over the past ~75 yr. (**Supplementary Figure S1**).

Uncalibrated radiocarbon dates range from 90 to 4,680 ^{14}C yr (**Table 2**). The paired dates on wood and sedimentary OM from the 40-cm horizon showed an offset of 4,220 yr. The absence of deep scour on seismic lines or within the core suggests that a sizable old carbon reservoir, rather than a major unconformity, is responsible for the offset in the paired

botanical-OM dates. The difference between these dates was therefore used as a correction factor for the other ^{14}C dates developed on acid-insoluble bulk OM. The reservoir-corrected ^{14}C dates ranged from 90–460 uncalibrated yr. BP. Integrating the $^{210}\text{Pb}_{\text{xs}}$, ^{137}Cs , and reservoir-corrected ^{14}C dates into a Bacon age-depth model indicates that core 9B spans 1654–2019 CE (~365 yr.) (**Figure 8**). The long-term sedimentation rate at the site is .16 cm/yr. Sedimentation rates within the ^{14}C -dated interval are .09 cm/yr., approximately five times slower than sediments accumulating within the interval constrained by $^{210}\text{Pb}_{\text{xs}}$ and ^{137}Cs dating.

Stratigraphy and Geochemistry

Core 9B was subdivided into four (I–IV, oldest to youngest) lithostratigraphic units on the basis of macroscopic features (e.g., sedimentary structures, density contrasts revealed in x-radiograph), sediment composition, MS, GRAPE, and geochemical trends (**Figure 8**). Along the length of the 57.5 cm core, TOC, TON, and C/N values ranged between ~1.09 and 2.85 wt. %, ~.13 to .38 wt. %, and ~8 to 14, respectively (**Figure 9**). All of the core sediments correlate with AF-1, the low-moderate amplitude, parallel, continuous reflections that are common in the deepwater depocenter.



Unit I (57.5–40.5 cm; ~1650–1840 CE)

Unit I sediments consist of light tan clayey silts with diatoms. Unit I is faintly laminated, with variably continuous planar or truncated, discontinuous laminations that produce density contrasts on the x-radiograph (Figure 8). Values of MS, GRAPE, and counts of Si, Al, K, Ti are higher than those characterizing the overlying units (Figure 9). TOC and C/N are uniformly low, with means of ~1.49 wt. % and 9 respectively. Counts of P and S are also relatively low in Unit I.

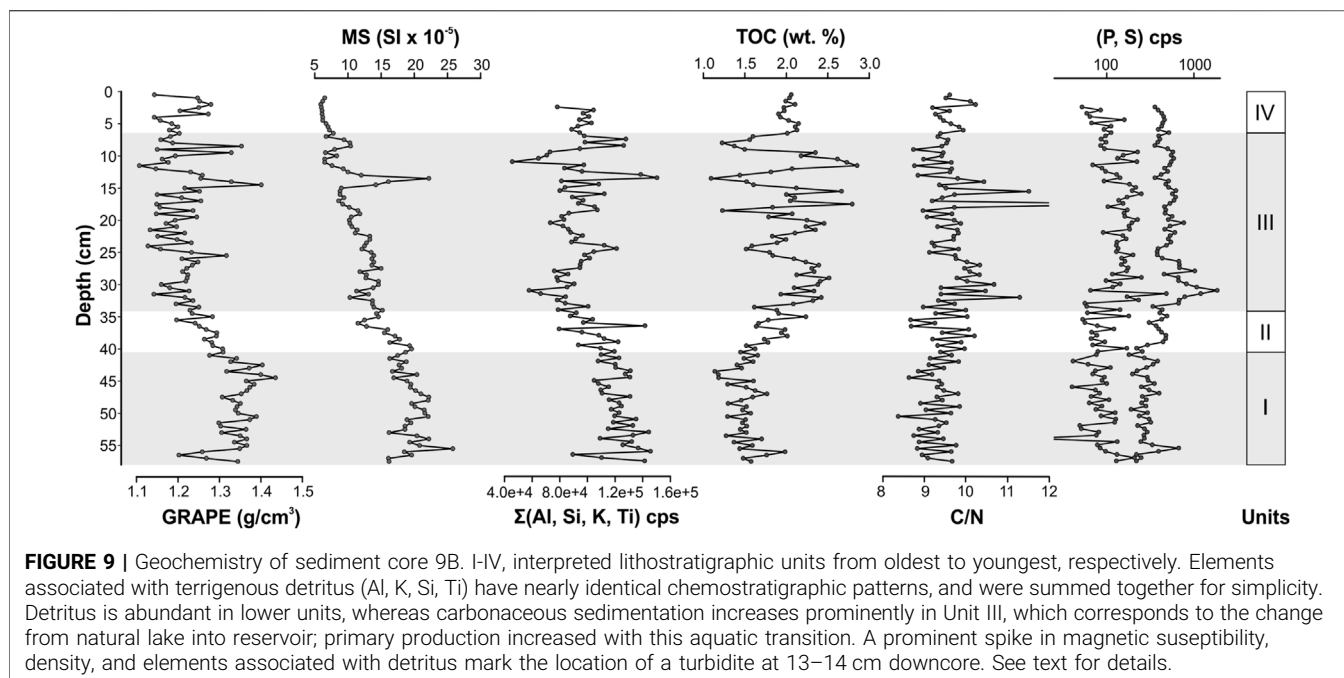
Unit II (40.5–34 cm; ~1840–1910 CE)

Unit II consists of dark tan laminated diatom-rich silt (Figure 8). Laminations in Unit II are typically planar, thin and continuous, although two thicker (3–4 mm) slightly undulose laminae are prominent in core photos and x-radiography (Figure 8). Unit II sediments exhibit a transition towards lower GRAPE values and higher TOC concentrations (mean of ~1.82 wt. %) relative to Unit I (Figure 9). MS, Si, Al, K, and Ti values decline across the basal contact and generally continue that trend towards the

upper contact, whereas C/N, P, and S show little variability relative to Unit I sediments.

Unit III (34–6.5 cm; ~1910–2003 CE)

Unit III consists of alternating bundles of thickly laminated, OM-rich, black diatomaceous ooze and light tan silty ooze (Figure 8). A cm-scale bed of normally graded light tan silt occurs at 13–14 cm downcore (~1986 CE), forming a prominent density contrast on the x-radiograph and a spiky response on the GRAPE, MS, and the detrital mineral-associated major elements (Figure 9). Following an initial increasing trend above the basal contact, high amplitude variability characterizes the TOC concentrations of Unit III, with a mean of ~2.03 wt. %. Black laminated oozes have the highest TOC, P and S values, whereas tan silty oozes show comparatively lower TOC but higher Al, Si, K, and Ti. C/N increases above the basal contact, then exhibits moderate variability around a mean of 10, including a set of peaks between 18 and 12.5 cm that are the maximum values in the core.



Unit IV (6.5–0 cm; ~2003–2019 CE)

Unit IV consists of dark tan, mostly structureless diatom-rich silt; occasional laminations are present on the x-radiograph. Unit IV exhibits uniform and relatively low MS, whereas GRAPE is variable (**Figure 9**). TOC and C/N are uniform and relatively high, with means of 2.03 wt. % and 10, respectively. Major element chemostratigraphic data for these sediments are unremarkable.

Statistical Analysis

Principal components analysis was performed on TOC, TN, MS, GRAPE, Al, Si, K, Ti, P and S (**Supplementary Figure S2**). The first principal component (PC1) explains ~63% of the variance, whereas all other components explain <15%. Positive loadings on PC1 were the detrital mineral-associated major elements, MS, and GRAPE, and negative loadings were on TOC, TN, P, and S. Therefore, the PC1 curve is interpreted as sediment composition, with positive values reflecting terrigenous detritus, and negative values reflecting carbonaceous sediments. The PC1 time series is dominated by positive values prior to dam completion (1908–1916 CE), though a multi-decadal transitional interval with oscillations between positive and negative values occurs beginning in the 1870s CE (**Figure 10A**). Negative values dominate the period following dam installation. Three short lived oscillations to positive values occurred in the 20th century: in the early 1960s, mid-late 1980s, and the late 1990s-early 2000s. These intervals occurred during lake level lowstands driven by climate change (Dilworth et al., submitted). A strong directional correspondence exists between Jackson Lake level elevation and core 9B TOC for the period following dam installation (**Figure 10B**).

DISCUSSION

Sublacustrine Geomorphology and Evidence of Dam Installation

Bathymetry, acoustic basement, and shallow acoustic facies data help to confirm inferences on the regional glacial and tectonic history made in previous investigations of Grand Teton National Park, as well as reveal novel aspects of the limnogeology of Jackson Lake (**Figures 4, 5**). The Teton fault imparts a first-order control on the availability of accommodation in the Jackson Hole basin (Byrd et al., 1994), and the deepwater depocenter of Jackson Lake approximately corresponds with the zone of maximum fault displacement identified by Thigpen et al. (2021). The topography created by the Teton Range organizes both the regional hydrology and weather patterns, and therefore the interaction of rivers and storms with Jackson Lake (Byrd et al., 1994) (**Figure 1**). That the major deepwater depocenter of Jackson Lake is situated adjacent to the Teton fault comes as little surprise, as fault-related subsidence considerably pre-dates Pleistocene glaciation and associated erosional scour (Licciardi and Pierce, 2018; Thigpen et al., 2021). Maximum water depth (~190 ms TWTT; ~143 m), maximum acoustic basement depth (~335 ms TWTT), and maximum sediment thickness (~150 ms TWTT) occur on the western side of the deepwater depocenter (**Figure 4**), and this feature defines both Jackson Lake's morphology and the spatial organization of acoustic facies. Unlike a number of hydrologically open half-graben lakes (e.g., Colman, 2006; McGlue et al., 2006), the basin fill of Jackson Lake does not appear to thicken preferentially towards the Teton fault,

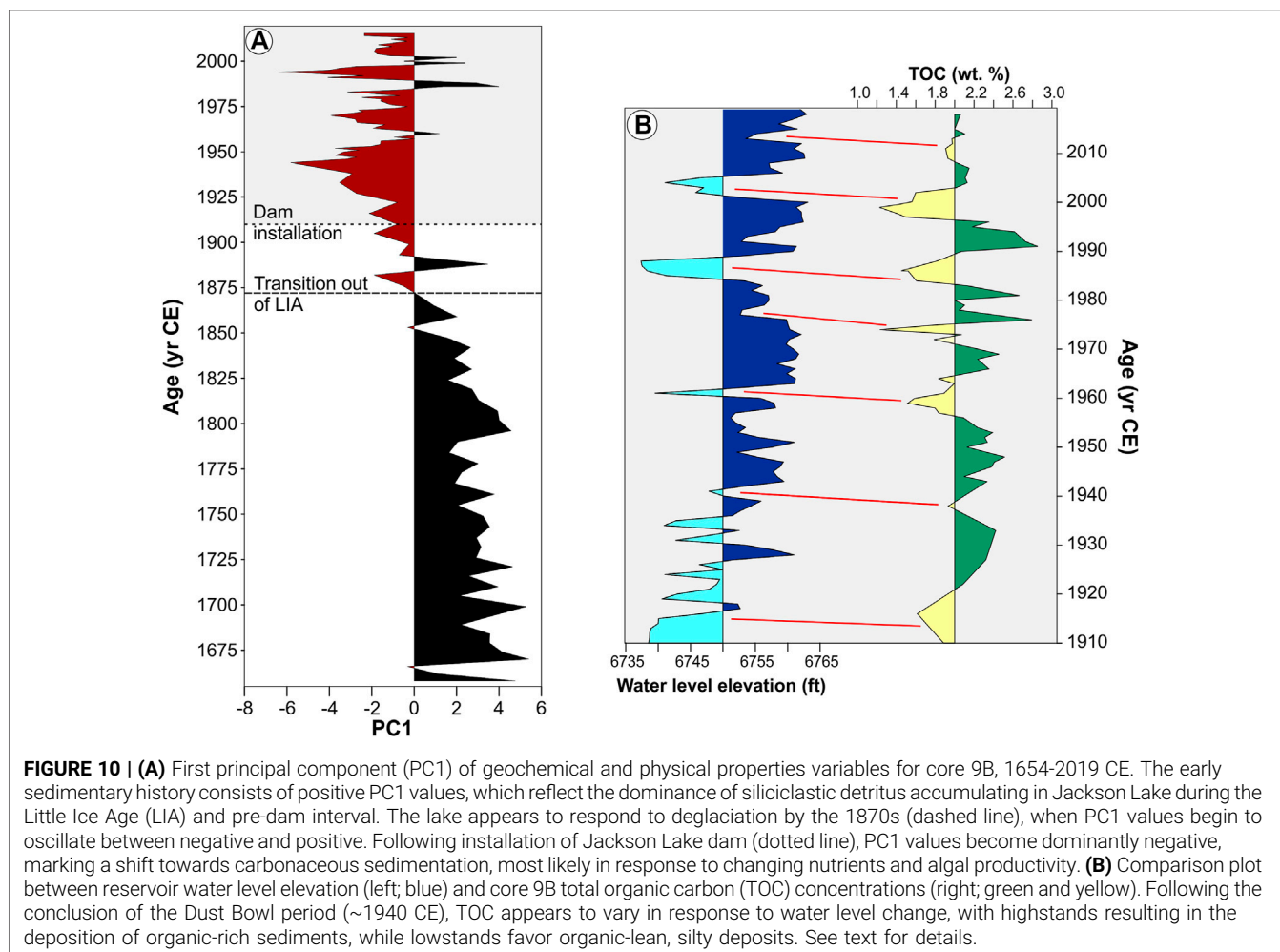


FIGURE 10 | (A) First principal component (PC1) of geochemical and physical properties variables for core 9B, 1654–2019 CE. The early sedimentary history consists of positive PC1 values, which reflect the dominance of siliciclastic detritus accumulating in Jackson Lake during the Little Ice Age (LIA) and pre-dam interval. The lake appears to respond to deglaciation by the 1870s (dashed line), when PC1 values begin to oscillate between negative and positive. Following installation of Jackson Lake dam (dotted line), PC1 values become dominantly negative, marking a shift towards carbonaceous sedimentation, most likely in response to changing nutrients and algal productivity. **(B)** Comparison plot between reservoir water level elevation (left; blue) and core 9B total organic carbon (TOC) concentrations (right; green and yellow). Following the conclusion of the Dust Bowl period (~1940 CE), TOC appears to vary in response to water level change, with highstands resulting in the deposition of organic-rich sediments, while lowstands favor organic-lean, silty deposits. See text for details.

supporting the interpretation that glacial activity played a key role in the organization of strata. Pierce and Good (1992) suggested that the southward directed Snake River lobe of the Yellowstone glacier system was responsible for scouring the Jackson Lake basin, and cosmogenic isotope dating of moraines indicates that the landscape formed between 16 and 13 ka (Licciardi and Pierce, 2018). Considerable acoustic variability characterizes the depocenter fill, and while the presumed age of Jackson Lake sediments aligns with the middle Pinedale phase, testing that hypothesis requires additional data that could be accessible with long coring technology (Harms et al., 2020). Importantly, few alpine or glacial lakes in the western USA contain similarly thick packages of syn- and post-glacial sediment (see Hofmann et al., 2006 for an exception), and the likelihood of rapid sedimentation hints at a unique and potentially high-resolution archive of environmental and tectonic change.

The dominant shallow acoustic facies in the dataset, AF-1, is interpreted to have formed from suspension settling of fine detritus, OM, and biochemical opal, as well as thin

gravity flows (Figure 5). This interpretation is supported by the lithostratigraphic units in core 9B, as well as the composition of grab samples from water ≥ 35 m deep (not shown). Seismic facies similar to AF-1 have been identified in many large lakes, with the km-scale continuity of low amplitude reflectors representing widespread gravitational settling of fine particulates (Colman, 2006; McGlue et al., 2008). Relief on AF-1 on the basin floor is often a consequence of underlying, acoustically chaotic mass wasting lobes that may have formed due to instability on the slope-forming faults that bound the depocenter (e.g., Figure 6C). CHIRP profiles reveal that thickness variations in AF-1 within shallow depositional environments most often occur as a function of relief generated by underlying glacial deposits, such as the mound-like drumlins on the eastern margin (AF-4) that formed during glacial retreat (Figure 3) (Pierce et al., 2018). The steep slope formed by the eastward facing, depocenter-bounding normal fault largely precludes the accumulation of lake sediments, and diffractions along this interface (AF-5) suggest exposed bedrock. This feature is tentatively

interpreted as an offshore expression of the Teton fault system.

Prograding clinoforms (AF-3) are interpreted as river deltas that were submerged and abandoned due to the installation of Jackson Lake dam and the transgression that followed (**Figure 7**). This interpretation is based on shallow stratal positions at the lake floor, the absence of extensive drape (as evidenced both on seismic profiles and sand-rich grab samples recovered from atop these features), and the position of the topset-to-foreset transition in all cases were ~11–12 m below the lake surface. Coarse-grained, Gilbert-type lacustrine deltas with characteristic topset, foreset, and bottomset beds are well-known in the geological record, with extensively studied examples from Great Salt Lake and its glacial predecessor, Lake Bonneville (e.g., Gilbert, 1890; Lemons et al., 1996). Oblique clinoforms with similar morphology to those in Jackson Lake have been seismically imaged in rift lakes and are routinely interpreted as paleo-deltas (e.g., Scholz et al., 1993; McGlue et al., 2006; Lyons et al., 2011). Reliable reconstruction of paleo-shoreline positions using submerged deltaic deposits makes the assumption that tectonic processes (fault initiation, isostatic rebound) did not significantly uplift/downdrop the clinoforms following deposition. In our data, evidence that could be used to argue against using the topset-to-foreset transition of the shallowest clinoforms as markers of water level was not found. Given the known magnitude of transgression associated with dam installation, the best interpretation of these features is as paleo-deltas of the Snake River, Arizona Creek, Moran Creek, and Pilgrim/Second Creek. The environment offshore of Arizona Creek was subaerially exposed in the 1980s, and surveyors speculated that a deltaic deposit was present, congruent with our interpretations (Connor, 1998). Importantly, the scale and thicknesses of these deltaic clinoforms precludes a more recent, inter-annual cycle of regression-transgression as the mechanism of formation; Patruno and Helland-Hansen (2018) suggest that clinoforms of this scale evolve over 10^2 – 10^5 years.

With the completion of Jackson Lake dam in 1916 CE, water level elevation steadily rose and exceeded 6,760 ft (2,060 m) asl by the late 1920s CE (**Figure 2**). Historical maps and satellite images show that much of the areal expansion of Jackson Lake occurred as flooding of the funnel-shaped Snake River valley. Therefore, the extensive AF-2 encountered in the northern lake axis is interpreted as submerged paleo-delta plain and paleo-lake margin environments that were created as the Snake River delta adjusted to higher base levels (**Figure 6A**). This interpretation aligns with the presence of incised channels observed on CHIRP profiles from the northern axis; these features are exposed during lake level lowstands today and collect the flow of the Snake River (**Figure 2C**). Clayey sands recovered in grab samples from the submerged channels suggest the potential for bedload transport and bypass of Snake River

sediments to the deepwater depocenter regardless of lake level elevation, as has been shown for other lakes (e.g., Soreghan et al., 1999). The flooding of the formerly subaerial and vegetated Snake River delta plain, as well as forested paleo-shorelines at the southern end of the lake, due to dam installation are interpreted to have influenced nutrient cycling and carbonaceous sedimentation in Jackson Lake.

Sediment Core Geochronology and Radiocarbon Reservoir Effects

^{137}Cs and $^{210}\text{Pb}_{\text{xs}}$ for core 9B confirm recent sedimentation rates (mean = .41 cm/yr.) in Jackson Lake reservoir are rapid with respect to radiocarbon-dated sediments from the same core, but are low-moderate in comparison to other reservoirs globally, a number of which accumulate sediment >.5 cm/yr (e.g., Miller and Heit, 1986; Whicker et al., 1994; Valero-Garcés et al., 1999; Stromsoe et al., 2016). Shuey et al. (1977) reported sedimentation rates in Jackson Lake derived from magnetic measurements on cores that ranged from .09 to .15 cm/yr. over the period 1175–1974 CE; one core (701-8) presented by these authors was collected in close proximity to core 9B. Shuey et al. (1977) also reported that 14 cm of silt had accumulated on the formerly subaerial Snake River plain from 1905 to 1974 CE, and suggested that dam installation was responsible for the inferred rapidity of accumulation (~.20 cm/yr.). The well-defined and reproducible ^{137}Cs peaks in both cores 9B and 10B (**Figure 8**; **Supplementary Figure S1**) suggest the early magnetic studies under-estimated post-dam sedimentation rates within Jackson Lake. The mechanisms responsible for rapid sedimentation in Jackson Lake are challenging to pinpoint with the available datasets. The ratio of Jackson Lake's surface area to the catchment area of the Snake River is relatively low (~.08) suggesting the potential for storage in upland landforms that might result in low sediment yield at the delta (e.g., Graf et al., 2010). However, much of the catchment consists of easily weathered volcanic and sedimentary highlands that have been sculpted by cycles of Pleistocene glaciation. The convergence of these conditions imply the potential for extensive mud production and transport in the source area (Potter et al., 2005). Seasonal carbonaceous and biochemical (opal) sedimentation, which have increased with dam installation, likely play a role as well. Additionally, winnowing of positive relief features on the lake floor may contribute sediments to the deepwater depocenter. Shallow water mounds (AF-4; interpreted as submerged drumlins or moraines) without draping low-amplitude reflections suggests that lacustrine sediments may have been removed from these positive-relief features (**Figures 6B, C**). Sediment focusing, the process by which waves or other currents remobilize fine-grained sub-littoral sediments and carries them offshore, is plausible for Jackson Lake due to the steep slope

along the eastern platform margin and the prevalence of intense wave turbulence during storms (e.g., Blais and Kalff, 1995).

The offset in ^{14}C age between terrestrial wood and acid-insoluble OM is considerable ($\sim 4,220$ yr.) for geologically young materials recovered from deepwater in Jackson Lake. The $\delta^{13}\text{C}$ measured on these samples are within $\sim 1.1\%$ (Table 2), suggesting contamination with exogenous sources is unlikely, and therefore a radiocarbon reservoir effect influences the basin. Reservoir effects occur when pre-aged dissolved carbon discharged from groundwater, delivered by rivers, emanated as hydrocarbons or upwelled from deep areas mixes with lake water in equilibrium with atmospheric CO_2 . Phytoplankton uptake of these diverse carbon sources during photosynthesis can result in spuriously old ^{14}C ages (Geyh et al., 1997; Yu et al., 2007). Geological Survey Professional Paper 110 (1978) noted the presence of hot springs near the northwestern lake shoreline, along the Teton fault trace. These springs were submerged with dam installation, and subsequently re-exposed when water levels were drawn down due to drought. The springs emerge from Mississippian-age limestones at 60°C – 72°C and pH of <6.8 , and an oil film was reported from one of the discharge zones. As a consequence, dissolved Paleozoic-aged carbon likely influences the ^{14}C reservoir in Jackson Lake. At present, the data available make it impossible to conclude if this reservoir effect varies temporally or spatially, as has been observed in some other large lakes (e.g., Felton et al., 2007; Oviatt, 2015). We therefore acknowledge that our approach to a reservoir correction has some inherent limitations, and we treat the mean modeled ages near the base of core 9B conservatively as maximum ages.

Lake Phase (Pre-Dam) Deepwater Sedimentation

Unit I encompasses the period in core 9B prior to marked water level changes and dam installation (~ 1650 – 1840 CE). The maximum lake water depth during Unit I was on the order of ~ 130 m, due to variably cold conditions over much of western Wyoming during this period. Diminished seasonality in Wyoming in the 17th–19th centuries is suggested by the growth of mountain glaciers (Schuster et al., 2000) associated with the Little Ice Age (LIA), a multi-century period of environmental change that has been registered by paleoclimate indicators across many northern Hemisphere sites (e.g., Mann et al., 2009). Abrasion of underlying bedrock associated with advancing glaciers in the region may be responsible for enhanced silt delivery to Jackson Lake during ice-free periods at this time. In the nearby Yellowstone National Park, blooms of *Stephanodiscus* diatoms in Crevice Lake suggest cold conditions and short summers between ~ 1150 and 1700 CE (Whitlock et al., 2008); Dilworth et al. (submitted) likewise noted abundant *Stephanodiscus* in

Unit I sediments. Oxygen isotopes measured on diatoms from Yellowstone Lake are compatible with a shift towards less evaporation and cold conditions after $\sim 1,000$ yr. BP (Brown et al., 2021). Tree ring studies from the Yellowstone ecosystem noted particularly cold conditions across ~ 1690 – 1709 and 1832 – 1851 CE (Rochner et al., 2021). Due to cold conditions of the LIA, lake ice was likely present into the summer months. Density contrasts between lake water and meltwater streams (dictated by temperature, salinity, and suspended sediment content) are important for lacustrine sedimentation affected by glaciers (Ashley, 2002). Diatoms from core 9B reveal that Unit I sediments were deposited when Jackson Lake's water column was relatively well-mixed, consistent with a cold paleoclimate (Dilworth et al., submitted). This suggests that density contrasts between Jackson Lake and its inflowing rivers may have been minor, and homopycnal flows dispersed fine-grained suspended sediments into the water column. The presence of planar continuous silty laminations are consistent with slow sedimentation (mean = $.09$ cm/yr.) by gravitational settling following flow dispersal (Figure 8). Contributions from underflows from the Snake River delta are likewise possible, given the variability in MS and the occasional presence of truncated laminae; silt delivered to deep glacial lake floors by this mechanism has been reported in the Swiss Alps (Sturm and Matter, 1978; Anselmetti et al., 2007). Organic content in Unit I sediments is low (mean TOC $<1.5\%$), chiefly consisting of algae (mean C/N = 9), and Jackson Lake was likely oligotrophic at this time (Figure 9).

Transitional Phase Deepwater Sedimentation

Unit II (~ 1840 – 1910 CE) marks a paleoenvironmental transition in Jackson Lake, witnessing the termination of the LIA and the inception of outlet engineering in the early 20th century. Proxy data from the region indicate that climate and landscape instabilities associated with the LIA ceased by 1850 – 1890 CE (e.g., Bracht et al., 2008; Heeter et al., 2021). Notably, the first marked transition in the PC1 dataset occurs in the 1870s CE (Figure 10A), demonstrating the sensitivity of Jackson Lake to regional paleoenvironmental conditions. The initial dam built on the Snake River outlet was a log and rock-filled crib structure that was completed by 1907, but subsequently failed in 1910. This structure increased the volume of Jackson Lake by $\sim 300,000$ acre-feet ($3.7 \times 10^8 \text{ m}^3$) (Stene, 1997). Unit II sediments exhibit a prominent shift toward lower GRAPE density values, and increasing trends in wt. % TOC and S cps shift the PC1 curve to negative values. Therefore, we interpret that Unit II marks the inception of biogenic sedimentation in the core 9B record. Laminated Unit II oozes are darker hues of tan in comparison to Unit I, which we posit reflects enhanced algal (C/N values are <10) production and preservation of OM. Two slightly undulose, light tan silty ooze laminae with low MS are prominent on the x-radiograph (Figure 8). One potential

interpretation for these features are dilute, distal turbidites that are aliased on the MS curve due to their thickness (3–4 mm). Alternatively, these laminae could be the result of eolian delivery of quartz-rich silt to the depocenter, with the absence of ferromagnetic grains responsible for low MS values. Given the steep slopes confining much of the depocenter, coupled with the shift towards a warmer climate, we favor the distal turbidite interpretation for these features.

Reservoir Phase (Post-Dam) Deepwater Sedimentation

Units III and IV (~1910–2019 CE) illustrate Jackson Lake's responsiveness to both dam installation and subsequent reservoir water level changes driven by regional drought and reservoir repairs. Completion of the dam in 1916 CE resulted in a major transgression generally, but particularly so northward, flooding the Snake River delta plain that is dominated by the AF-2 seismic facies, and drowning of paleo-deltas, islands, and glacial landforms with positive relief along the lateral margins (**Figures 2, 5**). Sedimentation in this period encompasses the Dust Bowl, a period of intense drought and warmer temperatures in the American West, which reduced streamflow on the Snake River (Cook et al., 2004; Wise, 2010). Reservoir water levels declined over several interannual periods in the 20th century due to drought, including the Dust Bowl (1930–1940 CE), 1959–1962 CE, 1984–1989 CE, and 2000–2009 CE (**Figure 2**), with significant ablation of Teton range glaciers occurring over this period (Edmunds et al., 2012). Notably, sediment accumulation in the corresponding intervals of core 9B was rapid, approximately five times faster than the rates of underlying units (**Figure 8**). Rapid sedimentation is not uncommon for reservoirs, as transgression results in wave reworking of previously subaerial environments, particularly during storms, yielding more sediment (e.g., Tibby et al., 2010).

A hallmark of Unit III deposits are interbedded bundles of OM-rich black and tan silty ooze laminae, which create high amplitude variability in wt. % TOC and a dominantly negative PC1 signal (**Figures 10A, B**). We interpret that dam completion and subsequent water level changes are responsible for the bedding-scale variability, while individual laminae composition is most likely reflective of seasonally contrasting depositional processes (e.g., autochthonous versus allochthonous sediment; Zolitschka et al., 2015). Talbot et al. (2006) noted that transgression can induce carbonaceous sedimentation in lakes due to alteration of nutrient budgets and a tendency towards stable chemical stratification as the water column deepens. Changes in nutrient status occur because flooding of lake margin environments drowns forest soils, trees, and supra-littoral wetlands, releasing nutrients into the lake; we infer this to have occurred in the northern axis of the lake and along southern shorelines.

Further, the combined effects of enhanced algal productivity (exploiting abundant nutrients) and the mineralization of terrestrial carbon can result in a relatively heavy oxygen demand that may induce periodic lake floor anoxia (Talbot et al., 2006). A shift toward mesotrophic conditions in Jackson Lake explains higher OM-content in deepwater sediments in Unit III, and the preservation of black laminae bundles is consistent with seasonal disoxia or anoxia, particularly when water levels were high. Dilworth et al. (submitted) observed a shift in diatom communities associated with Units III and IV, and interpreted these to reflect mesotrophic conditions and summer stratification of Jackson Lake. **Figure 10B** shows a strong directional correlation exists between wt. % TOC and reservoir water level elevation beginning in the late 1930s; slight offsets are most likely related to error associated with the age-depth model. The major departure from this trend occurs early in the reservoir history, as water levels varied considerably from 1920–1930 CE, in part due to Dust Bowl-related drought. Despite frequent regressions over that period, wt. % TOC increased (**Figure 10B**). This is best explained by processes in the early transgressive phase following dam completion in 1916 CE. We interpret the peaks in P and S, as well as the spiky response in C/N, to indicate decomposition of terrestrial vegetation and loading of Jackson Lake with a new source of nutrients that had a fertilizing effect on plankton, despite variability in water level (**Figure 9**). The diatom paleoecology presented in our companion paper supports this interpretation (Dilworth et al., submitted).

Although the PC1 dataset indicates that OM-rich sediments dominate following dam installation, there are three intervals (1960–1962 CE, 1986–1989 CE, and 2000–2002 CE) where values indicate transient shifts to siliciclastic detritus-dominated sedimentation. All three intervals align with lake level lowstands in Jackson Lake (**Figure 10B**). We interpret the normal grading, undulose capping layer, and abundant terrigenous detritus concurrent with the late 1980s lowstand to result from turbidite deposition. The characteristics of this bed are consistent with nearshore sediments that were carried downslope into deepwater, perhaps originating from an underflow on the Snake River delta (e.g., Praet et al., 2020; Vandekerckhove et al., 2020). Remobilization of previously deposited slope sediments due to pore pressure instabilities is an alternative source, but this possibility is less likely given the TOC signal (**Figure 9**). Notably, C/N are minimally changed through the turbidite, suggesting floods transporting terrestrial organic matter are unlikely. Limited evidence for flood-influenced sediments exists in Unit III sediments. The best candidate occurs during the lake level highstand of the late 1970s. A peak in C/N (~14) in 1976 CE (18 cm) corresponds with moderate MS and GRAPE values and high TOC, produced by mm-scale black and tan layers (**Figure 8**). A wildfire in Waterfalls Canyon occurred 1974 CE (Doyle et al., 1998), and it is plausible that post-

fire landscape instability resulted in a flushing effect of terrestrial OM when precipitation increased in subsequent years.

The last 16 years of the core 9B record (Unit IV) are characterized by relative stability in sediment chemistry and composition, with moderate-high TOC, low C/N, low MS, and moderate detrital mineral elemental abundances, consistent with relatively high water levels and hemipelagic sedimentation of algal OM and terrigenous silt (**Figure 9**). Variability in the GRAPE data and the absence of pervasive laminations could be a result of disruption of the upper few cm associated with entry of the gravity corer into the lake floor; variability in $^{210}\text{Pb}_{\text{xs}}$ is consistent with minor mixing in the upper few cm of both cores 9B and 10B. Alternatively, bioturbation could explain the absence of fine sedimentary structures, but we consider that interpretation less likely, given the OM preservation. Evidence of productivity driven bottom water anoxia or eutrophication are absent; diatoms studied by Dilworth et al. (submitted) demonstrate that recent shifts in trophic state or water quality have not accompanied the growing populations in the Jackson Hole Valley.

CONCLUSION

- (1) Jackson Lake, the largest glacial lake situated adjacent to the Teton fault in western Wyoming (USA), was transformed by the installation of a dam over the Snake River that was completed in the early 20th century. New CHIRP seismic reflection profiles and sediment cores collected from Jackson Lake reveal major changes to the lake system associated with rising base level following completion of the dam, and subsequent water level changes due to climate and water needs downstream. Seismic mapping of lake floor and acoustic basement horizons were used to produce bathymetric and isopach maps, clarifying basin morphology and the influence of faults and glacial erosion on water depth and sediment distribution patterns.
- (2) Five different shallow acoustic facies were identified across Jackson Lake, providing evidence for recent depositional processes and the effects of dam completion on lacustrine sedimentation. Prograding clinoforms, interpreted as paleo-deltas, occur offshore from the Snake River, Moran Creek, Arizona Creek, and Pilgrim/Second Creeks. These features, which occurred 11–12 m below the lake surface during the seismic survey, represent packages of coarse-grained sediment submerged beneath Jackson Lake that were abandoned with transgression. Flooding of the northern axis of Jackson Lake, once occupied by the Snake River delta plain, likely accounts for major changes in nutrient cycling that can be detected in deepwater sediment composition over the past century.
- (3) Deepwater sediments are readily dated using ^{137}Cs , ^{210}Pb , and ^{14}C , though a pronounced old carbon reservoir effect was discovered that influences age estimates from bulk OM in sediments older than ~100 years. Two cores recovered from the deepwater depocenter show largely comparable ^{137}Cs - and $^{210}\text{Pb}_{\text{xs}}$ -based age profiles and sediment accumulation rates; these data suggest that the pace of sedimentation accelerated five-fold following dam completion. Integration of all three geochronometers into a statistical age-depth model suggests that core 9B spans ~1654–2019 CE.
- (4) Sediment composition in deepwater showed marked sensitivity to environmental and anthropogenic changes to the lake system. Prior to ~1870 CE, sediments were silt dominated and occasionally laminated, likely a result of interaction between Jackson Lake and meltwater in the foreshortened ice-free seasons of the LIA. Dam installation shifted deposition to laminated carbonaceous oozes and silts. In the 20th century, high amplitude lake level changes controlled by droughts were directionally tracked by TOC concentrations. Instances of detritus-dominated sedimentation in the last century are restricted to periods of drought when Jackson Lake was at lowstand, which curtailed OM production or resulted in turbidite deposition. Sedimentary evidence demonstrates that the Jackson Lake ecosystem is sensitive to hydroclimate change and anthropogenic engineering, even in deepwater environments.

DATA AVAILABILITY STATEMENT

The original contributions presented in the study are included in the article/**Supplementary Material**, further inquiries can be directed to the corresponding author.

AUTHOR CONTRIBUTIONS

Project conceptualization—MM, RT, EW, and KY. Original draft—MM. Formal analysis—MM, JD, HJ, SW, EW, KY, RT, and SJ. Data visualization—MM, JD, HJ, KY, and SB. Project supervision—MM, RT, EW, and KY. Draft review and editing—All Authors. Data resources—All Authors. Methodology and laboratory facilities—MM, RT, KY, and EW. Project funding and management—RT, MM, EW, and KY.

FUNDING

This research was generously supported by the U.S. National Science Foundation Tectonics program (Award #1932808), the University of Wyoming-NPS field station, the Overcash Family Fund for Field Research, and the Pioneer Endowment at the University of Kentucky.

CONFLICT OF INTEREST

The authors declare that the research was conducted in the absence of any commercial or financial relationships that could be construed as a potential conflict of interest.

ACKNOWLEDGMENTS

Fieldwork for this project was conducted under permits NPS GRTE-2018-SCI-0060 and GRTE-2020-SCI-0049. We are grateful to the staff of the Colter Bay and Signal Mountain marinas for their willingness to facilitate our field operations. We appreciate SeisWare International Inc. providing academic licenses of their seismic interpretation software package SeisWare. We thank the Continental Scientific Drilling facility for core description, sampling and archival assistance. K. Schindler, R. Brown, J. Backus, E. Davis,

REFERENCES

- Anselmetti, F. S., Bühler, R., Finger, D., Girardclos, S., Lancini, A., Rellstab, C., et al. (2007). Effects of Alpine Hydropower Dams on Particle Transport and Lacustrine Sedimentation. *Aquat. Sci.* 69 (2), 179–198. doi:10.1007/s00027-007-0875-4
- Appleby, P. G., and Oldfield, F. (1983). The Assessment of ²¹⁰Pb Data from Sites with Varying Sediment Accumulation Rates. *Hydrobiologia* 103 (1), 29–35. doi:10.1007/bf00028424
- Ashley, G. M. (2002). “Glaciolacustrine Environments,” in *Modern and Past Glacial Environments* (Butterworth-Heinemann), 335–359.
- Blauuw, M., and Christen, J. A. (2011). Flexible Paleoclimate Age-Depth Models Using an Autoregressive Gamma Process. *Bayesian anal.* 6 (3), 457–474. doi:10.1214/11-ba618
- Blais, J. M., and Kalf, J. (1995). The Influence of Lake Morphometry on Sediment Focusing. *Limnol. Oceanogr.* 40 (3), 582–588. doi:10.4319/lo.1995.40.3.0582
- Bracht, B. B., Stone, J. R., and Fritz, S. C. (2008). A Diatom Record of Late Holocene Climate Variation in the Northern Range of Yellowstone National Park, USA. *Quat. Int.* 188 (1), 149–155. doi:10.1016/j.quaint.2007.08.043
- Brown, S. J., Thigpen, J. R., Spotila, J. A., Krugh, W. C., Tranel, L. M., and Orme, D. A. (2017). Onset Timing and Slip History of the Teton Fault, Wyoming: A Multidisciplinary Reevaluation. *Tectonics* 36 (11), 2669–2692. doi:10.1002/2016tc004462
- Brown, S. R., Cartier, R., Schiller, C. M., Zahajská, P., Fritz, S. C., Morgan, L. A., et al. (2021). Multi-proxy Record of Holocene Paleoenvironmental Conditions from Yellowstone Lake, Wyoming, USA. *Quat. Sci. Rev.* 274, 107275. doi:10.1016/j.quascirev.2021.107275
- Byrd, J. O., Smith, R. B., and Geissman, J. W. (1994). The Teton Fault, Wyoming: Topographic Signature, Neotectonics, and Mechanisms of Deformation. *J. Geophys. Res. Solid Earth* 99 (B10), 20095–20122. doi:10.1029/94jb00281
- Carroll, A. R., and Bohacs, K. M. (1999). Stratigraphic Classification of Ancient Lakes: Balancing Tectonic and Climatic Controls. *Geology* 27 (2), 99–102. doi:10.1130/0091-7613(1999)027<0099:scoalb>2.3.co;2
- Chopra, A. K. (1968). Earthquake Behavior of Reservoir-Dam Systems. *J. Eng. Mech. Div.* 94 (6), 1475–1500. doi:10.1061/jmcea3.0001050
- Christiansen, R. L. (2001). *The Quaternary and Pliocene Yellowstone Plateau Volcanic Field of Wyoming, Idaho, and Montana*. Reston, VA: USGS Professional Paper 729-G.
- Cintra-Buenrostro, C. E., Flessa, K. W., and Guillermo, A. S. (2005). Who Cares about a Vanishing Clam? Trophic Importance of *Mulinia Coloradoensis* Inferred from Predatory Damage. *Palaios* 20 (3), 296–302. doi:10.2110/palo.2004.p04–21
- Colman, S. M. (2006). Acoustic Stratigraphy of Bear Lake, Utah–Idaho—Late Quaternary Sedimentation Patterns in a Simple Half-Graben. *Sediment. Geol.* 185 (1–2), 113–125. doi:10.1016/j.sedgeo.2005.11.022
- Connor, M. A. (1998). *Final Report on the Jackson Lake Archeological Project: Grand Teton National Park, Wyoming (No. 46)*. Lincoln, NE: US Department of the Interior, National Park Service, Midwest Archeological Center.
- Cook, E. R., Woodhouse, C. A., Eakin, C. M., Meko, D. M., and Stahle, D. W. (2004). Long-term Aridity Changes in the Western United States. *Science* 306 (5698), 1015–1018. doi:10.1126/science.1102586
- Davies, S. J., Lamb, H. F., and Roberts, S. J. (2015). *Micro-XRF Studies of Sediment Cores*, 189–226. Micro-XRF Core Scanning in Palaeolimnology: Recent Developments
- Dilworth, J., Stone, J. R., Yeager, K. M., Thigpen, R. T., and McGlue, M. M. *Fossil Diatoms Reveal Natural and Anthropogenic History of Jackson Lake (Wyoming, USA)*. Earth Science Systems and Society. submitted.
- Doyle, K. M., Knight, D. H., Taylor, D. L., Barmore, W. J., and Benedict, J. M. (1998). Seventeen Years of Forest Succession Following the Waterfalls Canyon Fire in Grand Teton National Park, Wyoming. *Int. J. Wildland Fire* 8 (1), 45–55. doi:10.1071/wf9980045
- DuRoss, C. B., Zellman, M. S., Thackray, G. D., Briggs, R. W., Gold, R. D., and Mahan, S. A. (2021). Holocene Paleoseismology of the Steamboat Mountain Site: Evidence for Full-Length Rupture of the Teton Fault, Wyoming. *Bull. Seismol. Soc. Am.* 111 (1), 439–465. doi:10.1785/0120200212
- Edmunds, J., Tootle, G., Kerr, G., Sivanpillai, R., and Pochop, L. (2012). Glacier Variability (1967–2006) in the Teton Range, Wyoming, United States 1. *JAWRA J. Am. Water Resour. Assoc.* 48 (1), 187–196. doi:10.1111/j.1752-1688.2011.00607.x
- Felton, A. A., Russell, J. M., Cohen, A. S., Baker, M. E., Chesley, J. T., Lezzar, K. E., et al. (2007). Paleolimnological Evidence for the Onset and Termination of Glacial Aridity from Lake Tanganyika, Tropical East Africa. *Palaeogeogr. Palaeoclimatol. Palaeoecol.* 252 (3–4), 405–423. doi:10.1016/j.palaeo.2007.04.003
- Gawthorpe, R. L., and Leeder, M. R. (2000). Tectono-sedimentary Evolution of Active Extensional Basins. *Basin Res.* 12 (3–4), 195–218. doi:10.1111/j.1365-2117.2000.00121.x

SUPPLEMENTARY MATERIAL

The Supplementary Material for this article can be found online at: <https://www.escubed.org/articles/10.3389/esss.2023.10066/full#supplementary-material>

SUPPLEMENTARY FIGURE S1 | Comparative ²¹⁰Pb chronology for cores 9B (top) and 10B (middle). (Bottom) Core 10B ¹³⁷Cs and ²¹⁰Pb profiles with depth.

SUPPLEMENTARY FIGURE S2 | Biplot, principal components analysis for core 9B. PC1 explains ~63% of the variance among the different geochemical and physical properties and is interpreted as a representation of sediment composition. Positive values reflect abundant terrigenous detritus, whereas negative values reflect carbonaceous sedimentation.

- Geyh, M. A., Schotterer, U., and Grosjean, M. (1997). Temporal Changes of the 14C Reservoir Effect in Lakes. *Radiocarbon* 40 (2), 921–931. doi:10.1017/s0033822200018890
- Gilbert, G. K. (1890). *Lake Bonneville*, 1. Washington, DC: United States Geological Survey.
- Graf, W. L. (1999). Dam Nation: A Geographic Census of American Dams and Their Large-scale Hydrologic Impacts. *Water Resour. Res.* 35 (4), 1305–1311. doi:10.1029/1999wr900016
- Graf, W. L., Wohl, E., Sinha, T., and Sabo, J. L. (2010). Sedimentation and Sustainability of Western American Reservoirs. *Water Resour. Res.* 46 (12). doi:10.1029/2009wr008836
- Hammer, Ø., Harper, D. A., and Ryan, P. D. (2001). PAST: Paleontological Statistics Software Package for Education and Data Analysis. *Palaeontol. Electron.* 4 (1), 9. doi:10.1002/9780470750711
- Harms, U., Raschke, U., Anselmetti, F. S., Strasser, M., Wittig, V., Wessels, M., et al. (2020). Hipercorig—an Innovative Hydraulic Coring System Recovering over 60 M Long Sediment Cores from Deep Perialpine Lakes. *Sci. Drill.* 28, 29–41. doi:10.5194/sd-28-29-2020
- Heeter, K. J., Rochner, M. L., and Harley, G. L. (2021). Summer Air Temperature for the Greater Yellowstone Ecoregion (770–2019 CE) over 1, 250 Years. *Geophys. Res. Lett.* 48 (7). doi:10.1029/2020GL092269
- Hofmann, M. H., Hendrix, M. S., Moore, J. N., and Sperazza, M. (2006). Late Pleistocene and Holocene Depositional History of Sediments in Flathead Lake, Montana: Evidence from High-Resolution Seismic Reflection Interpretation. *Sediment. Geol.* 184 (1–2), 111–131. doi:10.1016/j.sedgeo.2005.09.019
- Johnson, S., Swallow, M., Thigpen, J. R., McGlue, M. M., Dortch, J., Gallen, S., et al. (2022). The Influence of Glacial Topography on Fluvial Efficiency in the Teton Range, Wyoming (USA). *Earth Planet. Sci. Lett.* 592, 117643. doi:10.1016/j.epsl.2022.117643
- Kilham, S. S., Theriot, E. C., and Fritz, S. C. (1996). Linking Planktonic Diatoms and Climate Change in the Large Lakes of the Yellowstone Ecosystem Using Resource Theory. *Limnol. Oceanogr.* 41 (5), 1052–1062. doi:10.4319/lo.1996.41.5.1052
- Kremer, K., Simpson, G., and Girardclos, S. (2012). Giant Lake Geneva Tsunami in AD 563. *Nat. Geosci.* 5 (11), 756–757. doi:10.1038/ngeo1618
- Larsen, D. J., Crump, S. E., Abbott, M. B., Harbert, W., Blumm, A., Wattrus, N. J., et al. (2019). Paleoseismic Evidence for Climatic and Magmatic Controls on the Teton Fault, WY. *Geophys. Res. Lett.* 46 (22), 13036–13043. doi:10.1029/2019gl085475
- Lemons, D. R., Milligan, M. R., and Chan, M. A. (1996). Paleoclimatic Implications of Late Pleistocene Sediment Yield Rates for the Bonneville Basin, Northern Utah. *Palaeogeogr. Palaeoclimatol. Palaeoecol.* 123 (1–4), 147–159. doi:10.1016/0031-0182(95)00117-4
- Licciardi, J. M., and Pierce, K. L. (2018). History and Dynamics of the Greater Yellowstone Glacial System during the Last Two Glaciations. *Quat. Sci. Rev.* 200, 1–33. doi:10.1016/j.quascirev.2018.08.027
- Ligon, F. K., Dietrich, W. E., and Trush, W. J. (1995). Downstream Ecological Effects of Dams. *BioScience* 45 (3), 183–192. doi:10.2307/1312557
- Love, J. D., Leopold, E. B., and Love, D. W. (1978). *Eocene Rocks, Fossils, and Geologic History, Teton Range, Northwestern Wyoming*. Washington, DC: United States: Department of the Interior, Geological Survey.
- Lyons, R. P., Scholz, C. A., Buoniconti, M. R., and Martin, M. R. (2011). Late Quaternary Stratigraphic Analysis of the Lake Malawi Rift, East Africa: An Integration of Drill-Core and Seismic-Reflection Data. *Palaeogeogr. Palaeoclimatol. Palaeoecol.* 303 (1–4), 20–37. doi:10.1016/j.palaeo.2009.04.014
- Maavara, T., Chen, Q., Van Meter, K., Brown, L. E., Zhang, J., Ni, J., et al. (2020). River Dam Impacts on Biogeochemical Cycling. *Nat. Rev. Earth Environ.* 1 (2), 103–116. doi:10.1038/s43017-019-0019-0
- Mann, M. E., Zhang, Z., Rutherford, S., Bradley, R. S., Hughes, M. K., Shindell, D., et al. (2009). Global Signatures and Dynamical Origins of the Little Ice Age and Medieval Climate Anomaly. *Science* 326 (5957), 1256–1260. doi:10.1126/science.1177303
- Marston, R. A., Mills, J. D., Wrazien, D. R., Bassett, B., and Splinter, D. K. (2005). Effects of Jackson Lake Dam on the Snake River and its Floodplain, Grand Teton National Park, Wyoming, USA. *Geomorphology* 71 (1–2), 79–98. doi:10.1016/j.geomorph.2005.03.005
- McGlue, M. M., Lezzar, K. E., Cohen, A. S., Russell, J. M., Tiercelin, J. J., Felton, A. A., et al. (2008). Seismic Records of Late Pleistocene Aridity in Lake Tanganyika, Tropical East Africa. *J. Paleolimnol.* 40 (2), 635–653. doi:10.1007/s10933-007-9187-x
- McGlue, M. M., Scholz, C. A., Karp, T., Ongodia, B., and Lezzar, K. E. (2006). Facies Architecture of Flexural Margin Lowstand Delta Deposits in Lake Edward, East African Rift: Constraints from Seismic Reflection Imaging. *J. Sediment. Res.* 76 (6), 942–958. doi:10.2110/jsr.2006.068
- Merritts, D., Walter, R., Rahnis, M., Hartranft, J., Cox, S., Gellis, A., et al. (2011). Anthropocene Streams and Base-Level Controls from Historic Dams in the Unglaciated Mid-Atlantic Region, USA. *Philosophical Trans. R. Soc. A Math. Phys. Eng. Sci.* 369, 976–1009. doi:10.1098/rsta.2010.0335
- Meyers, P. A., and Ishiwatari, R. (1993). Lacustrine Organic Geochemistry—An Overview of Indicators of Organic Matter Sources and Diagenesis in Lake Sediments. *Org. Geochem.* 20 (7), 867–900. doi:10.1016/0146-6380(93)90100-p
- Miller, K. M., and Heit, M. (1986). A Time Resolution Methodology for Assessing the Quality of Lake Sediment Cores that Are Dated by 137Cs. *Limnol. Oceanogr.* 31 (6), 1292–1300. doi:10.4319/lo.1986.31.6.1292
- Moernaut, J., Van Daele, M., Strasser, M., Clare, M. A., Heirman, K., Viel, M., et al. (2017). Lacustrine Turbidites Produced by Surficial Slope Sediment Remobilization: A Mechanism for Continuous and Sensitive Turbidite Paleoseismic Records. *Mar. Geol.* 384, 159–176. doi:10.1016/j.margeo.2015.10.009
- Nelson, N. C., Erwin, S. O., and Schmidt, J. C. (2013). Spatial and Temporal Patterns in Channel Change on the Snake River Downstream from Jackson Lake Dam, Wyoming. *Geomorphology* 200, 132–142. doi:10.1016/j.geomorph.2013.03.019
- Oviatt, C. G. (2015). Chronology of Lake Bonneville, 30,000 to 10,000 Yr BP. *Quat. Sci. Rev.* 110, 166–171. doi:10.1016/j.quascirev.2014.12.016
- Patrino, S., and Helland-Hansen, W. (2018). Clinoforms and Clinoform Systems: Review and Dynamic Classification Scheme for Shorelines, Subaqueous Deltas, Shelf Edges and Continental Margins. *Earth-Science Rev.* 185, 202–233. doi:10.1016/j.earscirev.2018.05.016
- Persico, L., and Meyer, G. (2013). Natural and Historical Variability in Fluvial Processes, Beaver Activity, and Climate in the Greater Yellowstone Ecosystem. *Earth Surf. Process. Landforms* 38 (7), 728–750. doi:10.1002/esp.3349
- Pierce, K., and Colman, S. (1986). Submerged Shorelines of Jackson Lake, Wyoming: Do They Exist and Define Postglacial Deformation on the Teton Fault. *UW Natl. Parks Serv. Res. Stn. Annu. Rep.* 10, 120–125. doi:10.13001/uwnpsrc.1986.2567
- Pierce, K. L., and Good, J. D. (1992). *Field Guide to the Quaternary Geology of Jackson Hole, Wyoming (No. 92-504)*. US Dept. of the Interior, US Geological Survey. doi:10.3133/ofr92504
- Pierce, K. L., Licciardi, J. M., Good, J. M., and Jaworowski, C. (2018). *Pleistocene Glaciation of the Jackson Hole Area, Wyoming (No. 1835)*. Reston, VA: US Geological Survey. doi:10.3133/pp1835
- Poff, N. L., Olden, J. D., Merritt, D. M., and Pepin, D. M. (2007). Homogenization of Regional River Dynamics by Dams and Global Biodiversity Implications. *Proc. Natl. Acad. Sci.* 104 (14), 5732–5737. doi:10.1073/pnas.0609812104

- Potter, P. E., Maynard, J. B., and Depetris, P. J. (2005). *Mud and Mudstones: Introduction and Overview*. Springer Science & Business Media.
- Praet, N., Van Daele, M., Collart, T., Moernaut, J., Vandekerckhove, E., Kempf, P., et al. (2020). Turbidite Stratigraphy in Proglacial Lakes: Deciphering Trigger Mechanisms Using a Statistical Approach. *Sedimentology* 67 (5), 2332–2359. doi:10.1111/sed.12703
- Reimer, P. J., Austin, W. E., Bard, E., Bayliss, A., Blackwell, P. G., Ramsey, C. B., et al. (2020). The IntCal20 Northern Hemisphere Radiocarbon Age Calibration Curve (0–55 Cal kBP). *Radiocarbon* 62 (4), 725–757. doi:10.1017/rdc.2020.41
- Rochner, M. L., Heeter, K. J., Harley, G. L., Bekker, M. F., and Horn, S. P. (2021). Climate-induced Treeline Mortality during the Termination of the Little Ice Age in the Greater Yellowstone Ecoregion, USA. *Holocene* 31 (8), 1288–1303. doi:10.1177/09596836211011656
- Sawakuchi, A. O., Hartmann, G. A., Sawakuchi, H. O., Pupim, F. N., Bertassoli, D. J., Parra, M., et al. (2015). The Volta Grande Do Xingu: Reconstruction of Past Environments and Forecasting of Future Scenarios of a Unique Amazonian Fluvial Landscape. *Sci. Drill.* 20, 21–32. doi:10.5194/sd-20-21-2015
- Schnurrenberger, D., Russell, J., and Kelts, K. (2003). Classification of Lacustrine Sediments Based on Sedimentary Components. *J. Paleolimnol.* 29 (2), 141–154. doi:10.1023/a:1023270324800
- Scholz, C. A., Johnson, T. C., and McGill, J. W. (1993). Deltaic Sedimentation in a Rift Valley Lake: New Seismic Reflection Data from Lake Malawi (Nyasa), East Africa. *Geology* 21 (5), 395–398. doi:10.1130/0091-7613(1993)021<0395:dsiarv>2.3.co;2
- Scholz, C. A., Rosendahl, B. R., and Scott, D. L. (1990). Development of Coarse-Grained Facies in Lacustrine Rift Basins: Examples from East Africa. *Geology* 18 (2), 140–144. doi:10.1130/0091-7613(1990)018<0140:docgfi>2.3.co;2
- Schuster, P. F., White, D. E., Naftz, D. L., and Cecil, L. D. (2000). Chronological Refinement of an Ice Core Record at Upper Fremont Glacier in South Central North America. *J. Geophys. Res. Atmos.* 105 (D4), 4657–4666. doi:10.1029/1999jd901095
- Sheriff, R. E. (1977). "Limitations on Resolution of Seismic Reflections and Geologic Detail Derivable from Them," in *Seismic Stratigraphy—Application to Hydrocarbon Exploration* (Tulsa, OK: AAPG Memoir), 26, 3–14.
- Shotbolt, L. A., Thomas, A. D., and Hutchinson, S. M. (2005). The Use of Reservoir Sediments as Environmental Archives of Catchment Inputs and Atmospheric Pollution. *Prog. Phys. Geogr.* 29 (3), 337–361.
- Shuey, R. T., Uglund, R. O., and Schmit, C. R. (1977). Magnetic Properties and Secular Variation in Cores from Yellowstone and Jackson Lakes, Wyoming. *J. Geophys. Res.* 82 (26), 3739–3746. doi:10.1029/jb082i026p03739
- Smith, R. B., Pierce, K. L., and Wold, R. J. (1993). "Seismic Surveys and Quaternary History of Jackson Lake, Wyoming," in *Geology of Wyoming: Wyoming Geological Survey Memoir*. Editors A. W. Snoke, J. R. Steidtmann, and S. M. Roberts, 5, 668–693.
- Snyder, N. P., Rubin, D. M., Alpers, C. N., Childs, J. R., Curtis, J. A., Flint, L. E., et al. (2004). Estimating Accumulation Rates and Physical Properties of Sediment behind a Dam: Englebright Lake, Yuba River, Northern California. *Water Resour. Res.* 40 (11). doi:10.1029/2004wr003279
- Soreghan, M. J., Scholz, C. A., and Wells, J. T. (1999). Coarse-grained, Deep-Water Sedimentation along a Border Fault Margin of Lake Malawi, Africa; Seismic Stratigraphic Analysis. *J. Sediment. Res.* 69 (4), 832–846. doi:10.2110/jsr.69.832
- Stene, E. A. (1997). *The Minidoka Project*. Denver, CO: Bureau of Reclamation History Program.
- Strasser, M., Monecke, K., Schnellmann, M., and Anselmetti, F. S. (2013). Lake Sediments as Natural Seismographs: A Compiled Record of Late Quaternary Earthquakes in Central Switzerland and its Implication for Alpine Deformation. *Sedimentology* 60 (1), 319–341. doi:10.1111/sed.12003
- Stromsoe, N., Marx, S. K., Callow, N., McGowan, H. A., and Heijnis, H. (2016). Estimates of Late Holocene Soil Production and Erosion in the Snowy Mountains, Australia. *Catena* 145, 68–82. doi:10.1016/j.catena.2016.05.013
- Sturm, M., and Matter, A. (1978). Turbidites and Varves in Lake Brienz (Switzerland): Deposition of Clastic Detritus by Density Currents. *Mod. Anc. lake sediments*, 147–168. doi:10.1002/9781444303698.ch8
- Talbot, M. R., Jensen, N. B., Lærdal, T., and Filippi, M. L. (2006). Geochemical Responses to a Major Transgression in Giant African Lakes. *J. Paleolimnol.* 35 (3), 467–489. doi:10.1007/s10933-005-2828-z
- Talbot, M. R. (2002). "Nitrogen Isotopes in Palaeolimnology," in *Tracking Environmental Change Using Lake Sediments* (Dordrecht: Springer), 401–439.
- Thigpen, R., Brown, S. J., Helfrich, A. L., Hoar, R., McGlue, M., Woolery, E., et al. (2021). Removal of the Northern Paleo-Teton Range along the Yellowstone Hotspot Track. *Lithosphere* 2021 (1), 1052819. doi:10.2113/2021/1052819
- Tibby, J., Gell, P., Hancock, G., and Clark, M. (2010). Complex Reservoir Sedimentation Revealed by an Unusual Combination of Sediment Records, Kangaroo Creek Reservoir, South Australia. *J. Paleolimnol.* 43 (3), 535–549. doi:10.1007/s10933-009-9349-0
- United States Geological Survey (1978). *Geological Survey Research 1978*. Washington, DC: U.S. Geological Survey. Professional Paper series 1100. 464. doi:10.3133/pp1100
- United States Geological Survey (1899). *Grand Teton Quadrangle. 1: 125000*. Washington, DC: U.S. Department of the Interior. N4330-W11030/30.
- Valero-Garcés, B. L., Navas, A., Machín, J., and Walling, D. (1999). Sediment Sources and Siltation in Mountain Reservoirs: a Case Study from the Central Spanish Pyrenees. *Geomorphology* 28 (1-2), 23–41. doi:10.1016/s0169-555x(98)00096-8
- Vandekerckhove, E., Van Daele, M., Praet, N., Cnudde, V., Haeussler, P. J., and De Batist, M. (2020). Flood-triggered versus Earthquake-triggered Turbidites: A Sedimentological Study in Clastic Lake Sediments (Eklutna Lake, Alaska). *Sedimentology* 67 (1), 364–389. doi:10.1111/sed.12646
- Waters, C. N., Syvitski, J. P., Galuszka, A., Hancock, G. J., Zalasiewicz, J., Cearreta, A., et al. (2015). Can Nuclear Weapons Fallout Mark the Beginning of the Anthropocene Epoch? *Bull. Atomic Sci.* 71 (3), 46–57. doi:10.1177/0096340215581357
- Whicker, J. J., Whicker, F. W., and Jacobi, S. (1994). ¹³⁷Cs in Sediments of Utah Lakes and Reservoirs: Effects of Elevation, Sedimentation Rate and Fallout History. *J. Environ. Radioact.* 23 (3), 265–283. doi:10.1016/0265-931x(94)90066-3
- White, B. J. P., Smith, R. B., Husen, S., Farrell, J. M., and Wong, I. (2009). Seismicity and Earthquake Hazard Analysis of the Teton-Yellowstone Region, Wyoming. *J. Volcanol. Geotherm. Res.* 188, 277–296. doi:10.1016/j.jvolgeores.2009.08.015
- Whitlock, C., Dean, W., Rosenbaum, J., Stevens, L., Fritz, S., Bracht, B., et al. (2008). A 2650-Year-Long Record of Environmental Change from Northern Yellowstone National Park Based on a Comparison of Multiple Proxy Data. *Quat. Int.* 188 (1), 126–138. doi:10.1016/j.quaint.2007.06.005
- Wise, E. K. (2010). Tree Ring Record of Streamflow and Drought in the Upper Snake River. *Water Resour. Res.* 46 (11). doi:10.1029/2010wr009282
- Xu, M., Dong, X., Yang, X., Wang, R., Zhang, K., Zhao, Y., et al. (2017). Using Palaeolimnological Data and Historical Records to Assess Long-Term Dynamics of Ecosystem Services in Typical Yangtze Shallow Lakes (China). *Sci. Total Environ.* 584, 791–802. doi:10.1016/j.scitotenv.2017.01.118
- Yeager, K. M., Santschi, P. H., and Rowe, G. T. (2004). Sediment Accumulation and Radionuclide Inventories (²³⁹, ²⁴⁰Pu, ²¹⁰Pb and ²³⁴Th) in the Northern Gulf of Mexico, as Influenced by

- Organic Matter and Macrofaunal Density. *Mar. Chem.* 91 (1-4), 1–14. doi:10.1016/j.marchem.2004.03.016
- Yu, S. Y., Shen, J., and Colman, S. M. (2007). Modeling the Radiocarbon Reservoir Effect in Lacustrine Systems. *Radiocarbon* 49 (3), 1241–1254. doi:10.1017/s0033822200043150
- Zolitschka, B., Francus, P., Ojala, A. E., and Schimmelmann, A. (2015). Varves in Lake Sediments—A Review. *Quat. Sci. Rev.* 117, 1–41. doi:10.1016/j.quascirev.2015.03.019

Publisher's Note: All claims expressed in this article are solely those of the authors and do not necessarily represent those of their affiliated organizations, or those of the publisher, the editors and the reviewers. Any product that may be evaluated in this article, or claim that may be

made by its manufacturer, is not guaranteed or endorsed by the publisher.

Copyright © 2023 McGlue, Dilworth, Johnson, Whitehead, Thigpen, Yeager, Woolery, Brown, Johnson, Cearley, Clark, Dixon, Goldsby, Helfrich, Hodelka, Lo, Domingos-Luz, Powell, Rasbold and Swanger. This is an open-access article distributed under the terms of the Creative Commons Attribution License (CC BY). The use, distribution or reproduction in other forums is permitted, provided the original author(s) and the copyright owner(s) are credited and that the original publication in this journal is cited, in accordance with accepted academic practice. No use, distribution or reproduction is permitted which does not comply with these terms.